$\gamma\gamma$ Event Generators

Conveners: Leif Lönnblad, Mike Seymour

Working group: Edouard Boudinov, Jon Butterworth, Ralph Engel, Alex Finch, Suen Hou, Maria Kienzle-Focacci, Mark Lehto, Ed McKigney, David Miller, Denis Perret-Gallix, Johannes Ranft, Gerhard Schuler, Torbjörn Sjöstrand, Rod Walker, Alison Wright.

Contents

1 Introduction

At LEP 2, two-photon collisions make up by far the largest class of events. These are processes in which the incoming electrons each radiate a photon, which collide to produce a hadronic or leptonic final state. A photon can obviously interact electromagnetically with any charged object. However, since it has the same quantum numbers as a vector meson, it can fluctuate into one, and can therefore also be considered as an incoming hadron, interacting strongly through its partonic constituents. The interplay between these two ways of interacting is unique to the photon and provides much of the interest in $\gamma\gamma$ physics.

The two-photon invariant mass spectrum is peaked at low mass, so the bulk of events only produce a few particles, and resonances and exclusive final states can be studied. The total cross-section is so large however, that there are enough events to study deep inelastic $e\gamma$ scattering and high-$p_\perp$ jets and heavy quark production in $\gamma\gamma$ collisions.

LEP 2 is the highest energy and luminosity $e\gamma$ and $\gamma\gamma$ collider available, and many of the same studies as at electron-hadron and hadron-hadron colliders can be made here. However, one essential difference is that, since the beam remnants (the electrons and positrons) typically leave the detectors undetected, the energies of the incoming photons are not known and must be reconstructed from the properties of the final state. In events in which most of the final-state particles are visible in the detector, this is easily done. However, at high energies the final-state distribution becomes increasingly forward-peaked and much of the energy goes into the very forward parts of the detector, or is even missed in the beam pipe. It is therefore essential that as much of the final state as possible is measured, in particular to detect hadrons in the forward detectors that have hitherto only been used for electron tagging.

It is also essential that we are able to understand the details of the multi-particle final states in these interactions, which puts very high demands on the event generators used in the analysis. During the course of this workshop, some of the standard general purpose event generator programs on the market have been developed to also handle $e\gamma$ and $\gamma\gamma$ collisions. This means that we can use our experience from ep and pp collisions to give a more complete description of the hadronic final state of two-photon collisions. These models can now be tested at LEP 1 and should give reliable extrapolations to LEP 2 energy.

In section 2 of this report, we will describe briefly the models of the generators we have studied during the workshop. Then, in section 3 some comparisons between the programs are presented for different classes of events. In section 4, the main programs are presented in some detail, followed by section 5 where some other generators are presented more briefly. Finally in section 6 we present our conclusions. Related work is presented in the reports of the "$\gamma\gamma$ Physics" [1] and "QCD Event Generator" [2] working groups.

2   General Features

The event generators used for $\gamma\gamma$ physics can be divided into two main groups. One deals with low multiplicity final states, like resonances, exclusive channels and leptonic channels and the other with high mass multi-particle final states.

When there are few particles in the final state, the fully differential cross-section for a given process can usually be derived directly from a model of that process. Event generators can then be viewed as a particularly convenient numerical implementation of that cross-section, in which arbitrarily complicated phase-space cuts and detector simulation can be incorporated. In this group are 'four-fermion generators', which incorporate the full set of QED matrix elements for $e^+e^- \rightarrow e^+e^-f\bar{f}$, and more general programs that use a $\gamma\gamma$ luminosity function to separate the process $e^+e^- \rightarrow e^+e^-X$ into two stages, $e^+e^- \rightarrow e^+e^-\gamma\gamma$ and $\gamma\gamma \rightarrow X$.

The other group of generators describe multi-particle production, for which cross-sections cannot be directly calculated in quantum mechanics. They use semi-classical probabilistic models to separate the process into several phases. First photons are radiated from the incoming electrons to give beams of quasi-real photons. Then a hard sub-process is generated, using partonic $2 \rightarrow 2$ matrix elements folded with the parton densities of the photon. The emission of additional partons from the incoming partons is generated by evolving them "backwards" in an initial-state parton shower, and from outgoing partons by generating a final-state parton shower. Finally, the partons are converted to hadrons, which are then allowed to decay.

2.1   Photon generation

A two-photon reaction can be factorized into photon fluxes of radiation from incoming $e^\pm$ and the final state of two-photon collisions. The decomposed differential cross-section for

$$e^+(p_1)e^-(p_2) \rightarrow e^+(p_1')e^-(p_2')\gamma(q_1)\gamma(q_2) \rightarrow e^+(p_1')e^-(p_2')X(q_1+q_2) \qquad (1)$$

is [3–5]

$$
\begin{aligned}
d\sigma \;=\; & \frac{\alpha^2}{16\pi^4 q_1^2 q_2^2}\left(\frac{(q_1q_2)^2 - q_1^2 q_2^2}{(p_1p_2)^2 - m_1^2 m_2^2}\right)^{1/2}\left(4\rho_1^{++}\rho_2^{++}\sigma_{TT} + 2|\rho_1^{+-}\rho_2^{+-}|\tau_{TT}\cos(2\tilde{\phi})\right. \\
& \left. +2\rho_1^{++}\rho_2^{00}\sigma_{TL} + 2\rho_1^{00}\rho_2^{++}\sigma_{LT} + \rho_1^{00}\rho_2^{00}\sigma_{LL} - 8|\rho_1^{+0}\rho_2^{+0}|\tau_{TL}\cos(\tilde{\phi})\right)\frac{d^3p_1'}{E_1'}\frac{d^3p_2'}{E_2'}, \;(2)
\end{aligned}
$$

where the σ's and τ's are linear combinations of the cross-sections for $\gamma\gamma \rightarrow X$ of transverse(T) and longitudinal(L) photons, the flux factor ρ_i^{ab} has photon helicities labelled by $+, -, 0$. Some dedicated $\gamma\gamma$ generators such as TWOGAM [6] use the full form of Eq. 2, while most models simplify further by taking the $q^2 \rightarrow 0$ approximation. At $q^2 \rightarrow 0$, the photons are quasi-real and transversely polarized and after integration over $\tilde{\phi}$, the angle between lepton scattering

planes, the only remaining term is σ_{TT}. Expressed in terms of a luminosity function we have

$$\sigma(e^+e^- \to e^+e^- X) = \frac{d^4\mathcal{L}_{\gamma\gamma}}{d\omega_1\,d\omega_2 d\theta_1 d\theta_2}\sigma_{TT}, \tag{3}$$

where $w_i = E_b - E_i'$ is the photon energy in the lab frame. The luminosity function can be decomposed as the product of a factor for each of the photons,

$$\frac{d^4\mathcal{L}_{\gamma\gamma}}{d\omega_1\,d\omega_2 d\theta_1 d\theta_2} = \frac{d^2\mathcal{L}_\gamma}{d\omega_1 d\theta_1}\frac{d^2\mathcal{L}_\gamma}{d\omega_2 d\theta_2}, \tag{4}$$

where, apart from a trivial kinematic factor, $d^2\mathcal{L}$ is the Equivalent Photon Approximation (EPA) flux factor,

$$\frac{d^2\mathcal{L}_\gamma}{d\omega d\theta} = 2p_t\,f(x, P^2), \tag{5}$$

with x the light-cone momentum fraction and P^2 the photon virtuality, $P^2 = |q^2|$. As discussed in Ref. [7], there are two important corrections to the usual EPA formula. The first is to include the sub-leading term of relative order m_e^2/P^2,

$$f_{\gamma/e}(x, P^2) = \frac{\alpha}{2\pi}\left(\frac{1 + (1-x)^2}{xP^2} - 2m_e^2\frac{x}{P^4}\right), \tag{6}$$

which can give corrections of order 10% for untagged and anti-tagged cross-sections. At present, of the QCD event generators, only PHOJET includes this correction. The second important correction is to include the correct, process-dependent, dynamic upper limit on P^2. However, this is only important for untagged cross-sections, and when an anti-tag condition is imposed, as it is throughout this report, this corrections become small.

2.2   Photon distribution functions

In resolved-photon processes we need parametrizations of the distribution functions for partons inside the photon. These obey an inhomogeneous form of the usual evolution equations. As discussed in more detail in the report of the "$\gamma\gamma$ Physics" working group [1], their solution can be written as the sum of a hadronic or VMD part, which evolves according the usual homogeneous equation, and a point-like or anomalous part.

There are a number of parametrizations available for the parton distribution functions of on-shell photons. Most of them are contained in a single package, PDFLIB [8], to which most of the event generators are interfaced. At present none use the recent models of the structure of virtual photons, although HERWIG does implement a simple P^2-suppression model. In the following when comparing different generators, we use the fairly similar SaS 1D [9] or GRV LO [10] sets.

4

direct	$\gamma\gamma \to q\bar{q}$
single resolved	$\gamma q \to qg$
	$\gamma g \to q\bar{q}$
double resolved	$qq' \to qq'$
	$gg \to q\bar{q}$
	$\vdots$
DIS	$eq \to eq$

Table 1: *The standard hard sub-processes used by event generators for different event classes*

2.3 Hard sub-processes

Having defined the structure functions and parton densities, we can now use the same machinery as for pp or ep collisions to generate hard sub-processes, with the exception that we here have additional processes where the photon couples directly in the hard interaction. In $\gamma\gamma$ collisions we therefore talk about three kinds of events, direct, single-resolved and double resolved, depending on whether the photons couple directly or not. In Table 1 the standard hard sub-processes are listed for different event classes. Some programs, like PYTHIA, make a further distinction between the anomalous and VMD–like part of the resolved photon and therefore have six different event classes.

In deep inelastic $e\gamma$ scattering, the exchanged photon is usually more virtual than the struck quark, so the EPA is no longer a good approximation (in other words the process-dependent dynamic upper limit on P^2 mentioned in Section 2.1 is exceeded). One therefore needs, in principle, to use the full $2 \to 3$ processes $eq \to eqg$, $eg \to eq\bar{q}$ and $e\gamma \to eq\bar{q}$. However, when the quark line is much less virtual than the photon, it can be approximated by the DGLAP probability distribution to find the quark inside a higher-x quark, $q \to qg$, gluon, $g \to q\bar{q}$ or photon, $\gamma \to q\bar{q}$ and hence can be absorbed into the evolution of the photon distribution functions. Thus we are again left with a $2 \to 2$ process, $eq \to eq$, for which one uses the lowest-order matrix element.

Other processes that are usually treated separately are the ones involving heavy quarks, where the matrix elements are different from the massless case. Here there are also event generators that use the next-to-leading order matrix elements, incorporating one additional parton. These can be considered as an exact treatment of the first step of a parton shower and can be compared with the usual algorithms discussed below, which contain approximate treatments of all steps.

5

2.4   Soft processes

The cross-section for quasi-real $\gamma\gamma$ scattering is dominated by processes in which there is no hard scale. Several models exist for the subdivision of the soft cross-section into separate components, typically: elastic, $\gamma\gamma \to VV$; single diffractive dissociation, $\gamma\gamma \to VX$; double diffractive dissociation, $\gamma\gamma \to XX$; and inelastic, $\gamma\gamma \to X$. The cross-section for each is given by the model, and the total cross-section is simply their sum. Clearly the separation is model specific, for example the difference between diffractive dissociation and inelastic scattering is the presence of a rapidity gap between the two systems in the former and not in the latter and the cross-sections depend on the size of this gap, and only the sum of the processes can be directly compared between models. Nevertheless, the available models use fairly similar definitions and comparisons between components can prove useful. Since most of these reaction types cannot be calculated from first principles, they are characterized by a rather large number of adjustable parameters. Nevertheless, since the models assume photon-hadron duality and hadron universality, parameters can be fixed in hadron-hadron and photon-hadron collisions, giving parameter-free predictions for LEP 2. PHOJET and PYTHIA contain rather complete soft interaction models, while HERWIG contains only the non-diffractive part of the cross-section.

2.5   Multiple interactions

At increasing centre-of-mass energies most sub-process cross-sections grow faster than the total cross-section, eventually overtaking it. Important examples include (supercritical) soft pomeron exchange and hard two-parton scattering above any given $p_{t\mathrm{min}}$ cut. This corresponds to the possibility of *multiple* soft or hard scatterings within a single $\gamma\gamma$ collision. At present only PHO-JET implements both soft and hard multiple scattering in the same package with $p_{t\mathrm{min}}$ forming the boundary between the two. PYTHIA and HERWIG (through an interface to the JIMMY generator) both implement multiple hard scattering above $p_{t\mathrm{min}}$, but with soft models that do not vary with $p_{t\mathrm{min}}$, so that it becomes a critical parameter of the model. Although the general ideas of the models are similar, there are many specific differences in their implementation. For example, the current models only allow multiple interactions in the hadronic cross-section, but since the definition of anomalous and hadronic events differs (see below), so do the multiple scattering results. In all three cases however, the models are essentially identical for $\gamma\gamma$ and γp collisions, so experience gained at HERA will certainly help constrain the predictions for LEP 2.

2.6   Parton showers

The hard scattering disturbs the colour fields of the incoming partons and as a result they partially 'shake off' the cloud of gluons that normally surrounds colour charges. This gives rise to a shower of accompanying radiation, which is conventionally modelled as a series of emissions from the incoming parton, starting from the parton entering the hard interaction and tracing

its history back towards the incoming photon. During this 'backwards evolution', the emission at each step is required to be at a lower scale than the previous one until, near the incoming photon, no more radiation is resolvable above the infrared cutoff. This procedure is governed by the splitting functions of the DGLAP evolution equation and is guided by the input set of parton distribution functions.

This is the way it is done in the two standard generators HERWIG and PYTHIA where the main difference between the two is the choice of evolution, or ordering variable – PYTHIA uses the virtuality of the evolving parton, while HERWIG uses a generalized emission angle, which incorporates colour-coherence effects.

Another important difference between the two programs is the way they distinguish between the anomalous and VMD–like part of the structure functions. In PYTHIA this distinction is done beforehand, and the shower is identical in both cases, only using different parton densities corresponding to the two parts of the structure functions. In HERWIG, however, the two parts are treated together, and an additional branching is introduced into the parton shower, where a quark may be evolved back to the incoming photon. If this happens before the shower is cut off, the event is called anomalous, if not, it is a VMD–like event. In both cases, the photon remnant will have a larger transverse momentum in the anomalous case — this is automatic in the perturbative treatment of HERWIG, while in PYTHIA it is put in by hand.

In both programs the generated partons may continue to branch in a final-state shower, in the same way as is done in e^+e^- annihilation. This is discussed in more detail in the report from the "QCD generator" group [2].

In contrast to HERWIG and PYTHIA, which use backward-evolution algorithms, the GGPS1 and GGPS2 programs evolve forwards, i.e. upwards in scale toward the hard process. This has the advantage that the evolution of the structure function is generated by the Monte Carlo algorithm itself, allowing a non-trivial test, whereas backward evolution is guaranteed to reproduce whatever distribution function is input. Like most implementations of forward evolution, GGPS1 and GGPS2 produce weighted events, which can be inconvenient for detector simulation. Forward evolution can also be extremely inefficient, particularly at small x, but this problem is solved in GGPS1 and GGPS2, as described in Section 4.3.

In the Dipole Cascade Model, implemented in the ARIADNE program, there is no explicit initial state radiation. Instead, in DIS, all gluon emissions are described in terms of dipole radiation from the colour dipole between the struck quark and the photon remnant. The radiation is suppressed in the remnant direction because of its spatial extension.

2.7   Hadronization

The hadronization of the produced partons is done according to the Lund string fragmentation model [11] except in HERWIG, where a cluster fragmentation model is used [12]. Both these models are explained in detail in the report from the "QCD generator" group [2].

The difference in hadronization between $\gamma\gamma$ and e^+e^- events is the presence of the photon remnant in the former. In PYTHIA the remnant is taken to be a single parton (optionally quark and an antiquark in case a gluon is taken out of the photon) which is treated like any other parton. In HERWIG, however, the cluster containing the remnant is treated a bit differently from the others as described in section 4.4.

The hadrons are subsequently decayed. Those produced by the hadronization process are generally taken to be unpolarized and thus decay according to pure phase-space, with standard decay tables as described in Ref. [2]. On the other hand, when vector mesons are produced elastically they are strongly transverse polarized, so they are decayed accordingly, with the two pions predominantly taking similar energies.

3   Comparisons

In the following, we will compare the predictions for LEP 2 of different generators for different kinds of processes. Unless specified otherwise, comparisons are made on the generator level, using a beam energy of 87.5 GeV, a total integrated luminosity of 500 pb^{-1} and requiring at least an invariant mass of 2 GeV of particles in the region $|\cos\theta| < 0.97$.

3.1   Exclusive channels and resonances

Lepton pair production, $e^+e^- \rightarrow e^+e^-\ell^+\ell^-$ is well described by the exact matrix elements, which are dominated by the multiperipheral diagram. In terms of the luminosity function, the lepton pair production is given by the QED structure function for $\gamma\gamma \rightarrow \ell^+\ell^-$. We have compared muon pair production by PC [13] applying the luminosity function to the exact calculations of matrix elements by DIAG36 [14] and Vermaseren [15]. The mass threshold imposed on the pair is $W > 300$ MeV. The distributions of $Q^2 = \max(-q_1^2, -q_2^2)$ and W obtained are shown in Fig. 1.

The cross-section of $\gamma\gamma \rightarrow R$ for a narrow resonance of spin-J is given by [3, 16]

$$\sigma(\gamma\gamma \rightarrow R) = 8\pi(2J+1)F^2(q_1^2, q_2^2)\frac{\Gamma_{\gamma\gamma}\Gamma}{(m_R^2 - W^2)^2 + m_R^2\Gamma^2}. \tag{7}$$

Here the resonance has mass m_R, radiative width $\Gamma_{\gamma\gamma}$, and energy dependent width Γ. For a wide resonance the Breit-Wigner term of Eq. 7 is multiplied by $(m_R/W)^n$ [16], with n=1,2 for the resonance decaying into two, three stable particles respectively. The q^2 dependence is given by the form factor function that satisfies $F^2(0,0) = 1$. The VMD model predicts

$$F^2(q_1^2, q_2^2) = \sum_{V_1, V_2} \frac{A_{V_1}}{(1 - q_1^2/m_{V_1}^2)^2} \frac{A_{V_2}}{(1 - q_2^2/m_{V_2}^2)^2}, \qquad \sum_V A_V \equiv 1, \qquad V = \rho, \omega, \phi, J/\psi \ldots \tag{8}$$
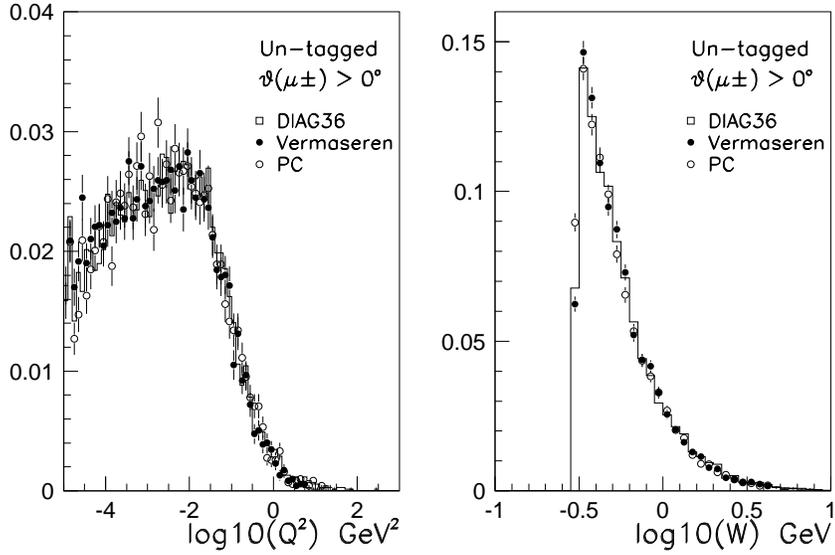
Figure 1: *The Q^2 and W distributions of $e^+e^- \rightarrow e^+e^-\mu^+\mu^-$ at $\sqrt{s} = m_z$.*
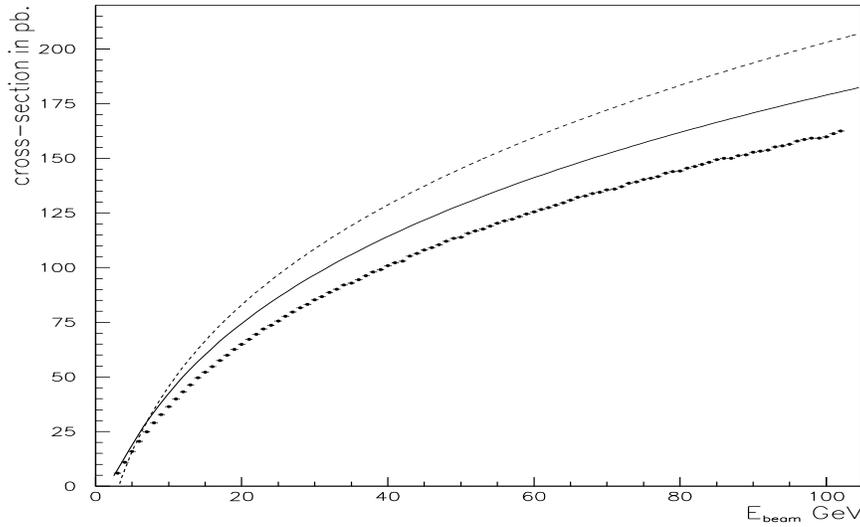

Figure 2: *The η_c cross-section versus beam energy: Low approximation, dashed; narrow-width approximation, solid;* RESPRO *results, points.*

In generating two-photon resonances, the mass spectrum is the product of the Breit-Wigner distribution and the two-photon invariant mass spectrum obtained from the luminosity function. The decay products are further described by the matrix element according to the spin-parity and helicity state that couple to the angular distributions of the final state particles.
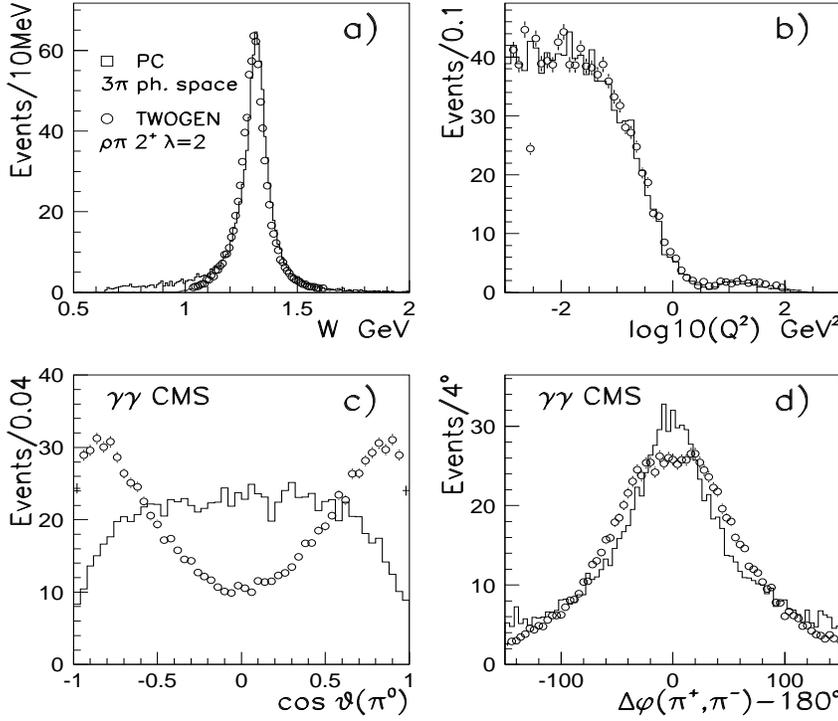
Figure 3: *The $a_2(1320)$ simulations of PC in 3π phase space and* TWOGEN *with J^P=2$^+$, helicity λ=2 and intermediate state $\rho\pi$. Detector acceptance are set to $\theta > 10°, 25°$ for calorimeter and central tracker respectively.*

We have compared the cross-section generated for η_c resonance as a function of beam energy which is shown in Fig. 2. The dashed line is the Low approximation [17] (i.e. the narrow-width approximation and the leading term of the EPA, but with the x-dependence of the P^2 integration neglected: $\int dP^2/P^2 \to \log s/m_e^2$), the solid line is the luminosity function of Eq. 2 using the approximation of $W^2 = 4w_1w_2$ for small q^2, and the points are the RESPRO [18] calculation using exact w_1w_2 without form factor.

We have instrumented the photon flux generated by PC and TWOGEN [19] to simulate $a_2(1320)$ mesons in $\pi^+\pi^-\pi^0$ final states at LEP 1 with detector acceptance set to $\theta > 10°, 25°$ from the beam direction for calorimeter and central tracker respectively. Shown in Fig. 3a and b are the invariant mass and Q^2 distributions of $a_2(1320)$ generated by PC and TWOGEN. Instrumented in PC is a narrow resonance of Eq. 7 decaying into 3π phase space, while in TWOGEN the Breit-Wigner of a wide resonance is multiplied by a matrix element of J^P=2$^+$ with helicity λ=2 and intermediate state of $a_2 \to \rho\pi \to \pi^+\pi^-\pi^0$. A second Breit-Wigner term for ρ suppresses events at low W. Within the detector acceptance good agreement is seen. The coupling to spin-parity and helicity state is demonstrated in Fig. 3c and d in which the π^0 distribution in polar angle and acollinear azimuthal angle of the two charged pion tracks are compared with the phase space distributions of PC.
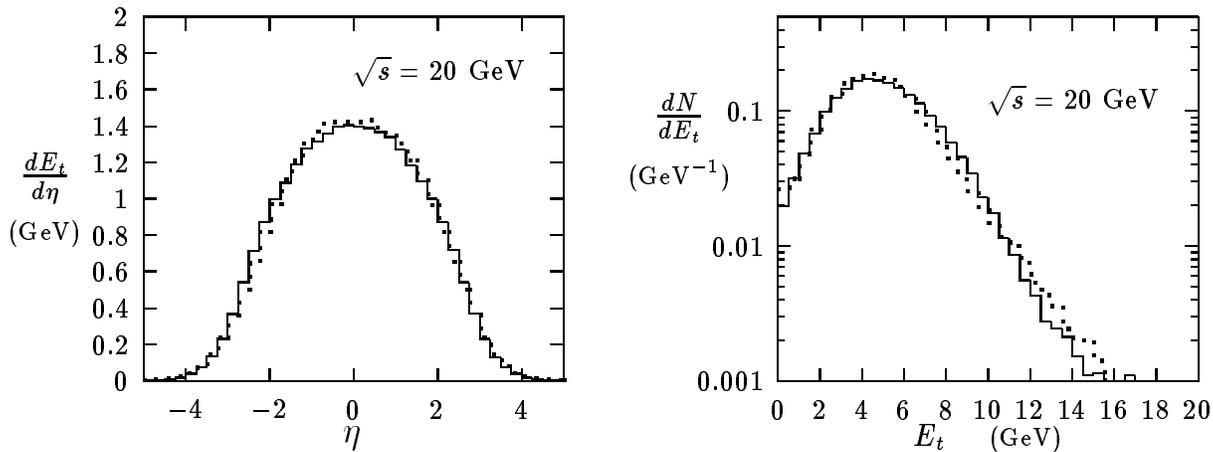
10

Figure 4: *Transverse energy flow and transverse energy distribution for photon-photon colli-sions. The full (dotted) line presents the predictions by* PYTHIA *(*PHOJET*).*
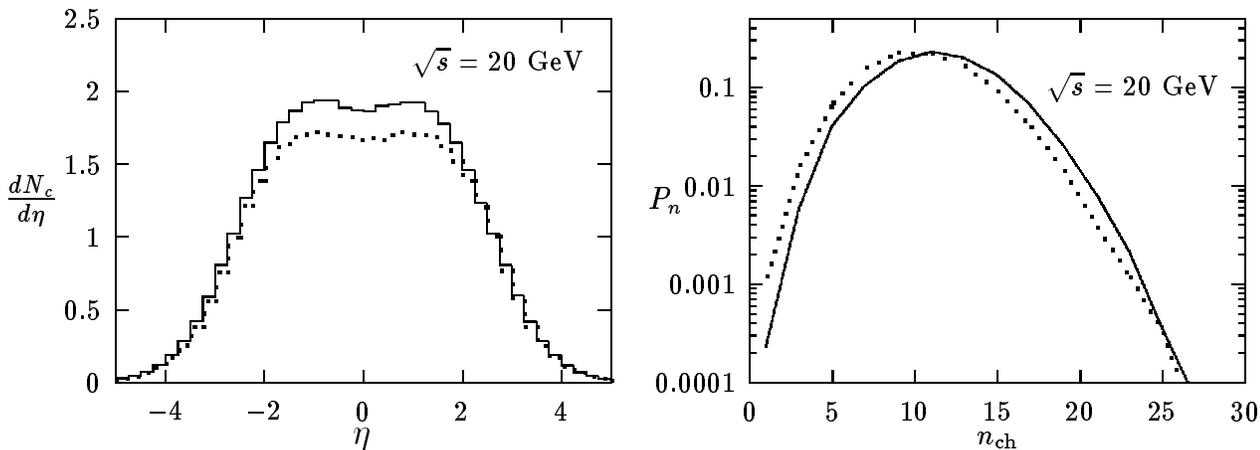

Figure 5: *Pseudorapidity distribution of charged particles and multiplicity distribution for non-single diffractive photon-photon collisions. The full (dotted) line presents the predictions by* PYTHIA *(*PHOJET*).*

3.2   Minimum bias events

In the following, some predictions for photon-photon collisions of the two minimum bias gener-ators PYTHIA and PHOJET are compared at fixed photon-photon energy. The calculations have been done for inelastic, non-diffractive events, using the photon parton distribution functions SaS 1D [9] (PYTHIA) and GRV LO [10] (PHOJET). The transverse energy is one of the typical minimum bias quantities which can be measured without collecting very high statistics. In Fig. 4a the transverse energy flow as function of the pseudorapidity is shown. The transverse energy distribution is shown in Fig. 4b. Both generators give similar predictions.

In Fig. 5a the charged particle distribution as function of the particle pseudorapidity is
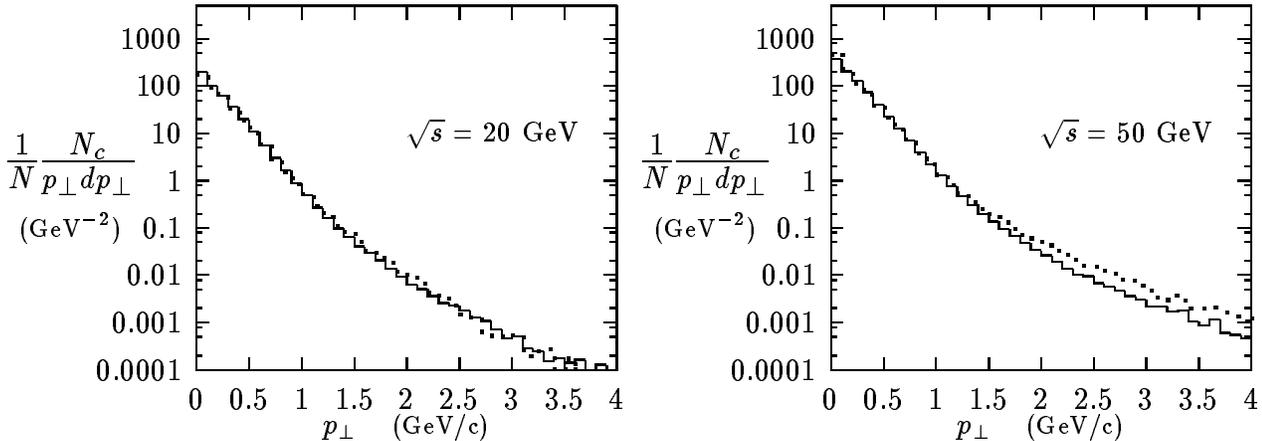
Figure 6: *Transverse momentum distributions of charged particles predicted by* PYTHIA *(full line) and* PHOJET *(dotted line).*

shown. PYTHIA predicts a higher charged particle density than PHOJET. This can be compared to the experimental value $dN_{ch}/d\eta = 1.4 \pm 0.1$ for inelastic proton-proton collisions [20] at $\sqrt{s} = 24$ GeV. The shapes of the charged particle multiplicity distribution calculated with the generators (shown in Fig. 5b) are similar, however PHOJET predicts a lower value for the average multiplicity.

In general PYTHIA gives a larger difference between $\gamma\gamma$ and pp (and γp) collisions than PHOJET but this discrepancy is expected to diminish once both programs have been properly tuned to HERA data.

Finally, the transverse momentum distribution of charged particles is shown in Fig. 6. Whereas at low energies the generator results agree, PHOJET predicts at $\sqrt{s} = 50$ GeV more charged particles at high transverse momentum than PYTHIA.

3.3 Deep inelastic scattering

When measuring the photon structure function in deep inelastic eγ scattering, it is of course necessary to be able to accurately measure the Q^2 and the Bjorken-x in each event. The Q^2 is easily obtained from the energy and angle of the scattered electron, but since the energy of the target photon is unknown, x must be determined from the hadronic final state. Thus one measures the distribution of visible hadronic mass, W_{vis}, and hence $x_{vis} \equiv Q^2/(W_{vis}^2 + Q^2)$. This is then converted into the distribution of x using an unfolding procedure, typically based on Refs. [21] or [22].

It is clear that the more of the solid angle over which we detect hadrons, the better correlated W_{vis} will be with the true hadronic mass, W_{true}, so the less work the unfolding procedure will have to do. For now we simply define W_{vis} to be the total invariant mass of all the hadrons

12

(a)

(b)

$dE_\perp/d\eta$ (GeV)

PYTHIA ——
ARIADNE - - -
HERWIG ....

3

2

1

0

-3 -2 -1 0 1 2 3

η

$\langle W_{\mathrm{vis}} \rangle$

PYTHIA ——
ARIADNE - - -
HERWIG ....

20

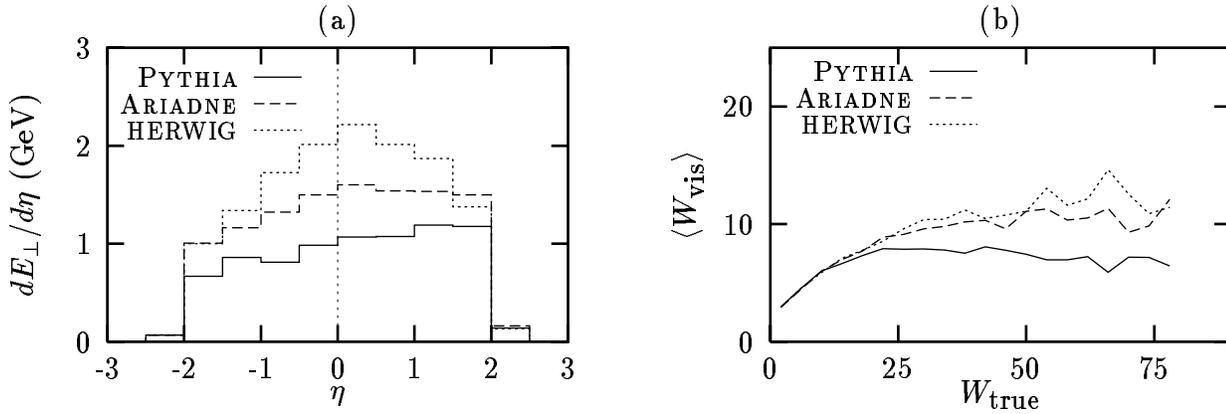10

0

0   25   50   75

W_{true}

Figure 7: *(a) The transverse energy flow in deep inelastic $e\gamma$ scattering at LEP 2 as predicted by different generators for $x < 0.01$. (b) The mean value of W_{vis} as a function of W_{true} at LEP 2 as predicted by different generators.*

within the angle covered by the tracking system of a typical LEP detector, $|\cos\theta| < 0.97$, as done in most previous analyses, and return to this point later.

The unfolding procedure relies heavily on the event generator's ability to correctly model the hadronic final state. In previous analyses (see for example Refs. [23,24]), the consistency of the generators used for the unfolding has been checked using inclusive distributions of the data, such as the distributions in Q^2, W_{vis} and particle multiplicity and momentum distributions. The problem is that such distributions can be fitted with basically any generator by adjusting the number of events in each x and Q^2 bin, i.e. by modifying the input parton distribution. To really check the generator's description of the final states, one needs to investigate less inclusive distributions.

Experience from HERA shows that at small x, the distribution of transverse energy, $E_\perp$, in the proton direction is very difficult to describe. Indeed, programs with conventional "DGLAP-like" initial-state parton showers cannot explain the measured $E_\perp$ perturbatively and are dominated by the non-perturbative components. On the other hand, the dipole cascade in the ARIADNE program describes the $E_\perp$ flow rather well at the perturbative level, with only small hadronization corrections. While more detailed measurements might hope to distinguish them, the most recent versions of all models are in good agreement with current data.

In Fig. 7a we show the $E_\perp$ flow for small-x events at LEP 2 predicted by some event generators. The reach in x is not as large as at HERA, but the differences are still large. In the forward and central regions, the differences are mostly due to the fact that HERWIG corrects the hardest emission to reproduce the full $\mathcal{O}(\alpha^2\alpha_S)$ and $\mathcal{O}(\alpha^3)$ matrix elements, while this is only done partly in ARIADNE and not at all in PYTHIA. In the backward (photon remnant) direction, PYTHIA is expected to be lower than ARIADNE because of the differences in the parton showers as explained above. HERWIG is here higher than PYTHIA due to the special treatment of the remnant fragmentation.
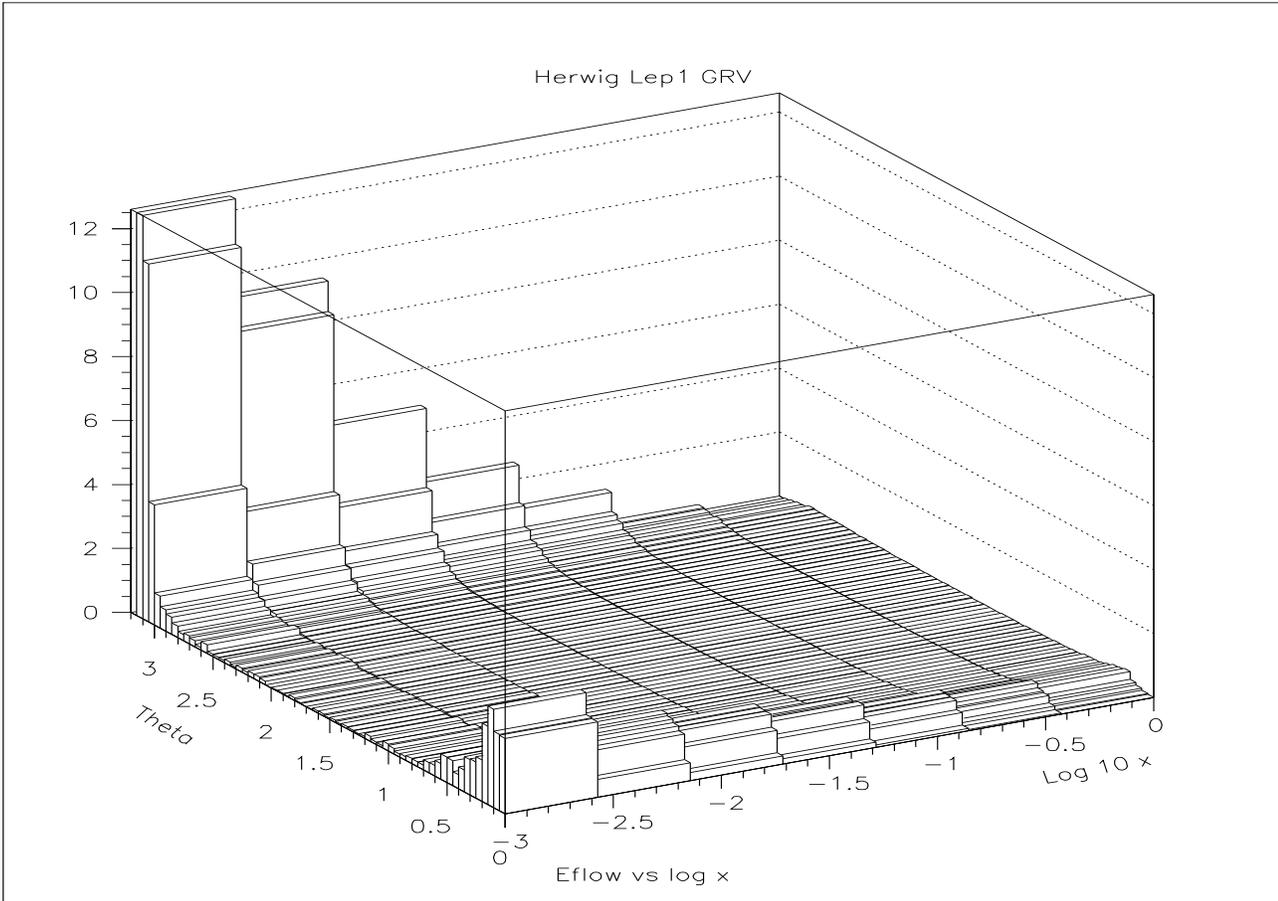
13

Figure 8: *The angular distribution of energy flow as a function of x at LEP 1 as predicted by HERWIG for events with $4 < Q^2 < 30$ GeV^2. The axes are such that the tagged electron is always on the forward, $0°$ side, while the photon remnant goes in the backward direction.*

It is clear that the relationship between W_{vis} and W_{true} is closely related to the energy flow, and in Fig. 7b we see that the models that give higher $E_\perp$ flow also give a stronger correlation between W_{vis} and W_{true} as expected. Also, all models predict a very weak correlation at large W_{true}, because more and more of the photon remnant falls outside the assumed acceptance as x gets smaller. This is demonstrated more clearly in Fig. 8, where the angular distribution of energy flow as a function of x is shown for LEP 1. The situation is even more extreme at LEP 2. The amount of energy falling into the central regions of the detector hardly increases with W, while almost all the increase is concentrated in the far forward and backward regions.

Our assumed detector acceptance covers all but the last five bins at each end, but we see that this is where most of the energy increase lies. However, all the LEP experiments have detectors in this region, which are used to tag electrons, and cover all but the very last bin of this plot. Thus if these could be used, even just to sample some of the hadronic energy in this region, a greatly improved W measurement could be made. Preliminary studies indicate

14

that in addition to the neutral pions, which can be measured because they decay to photons, a significant fraction of charged pions deposit some of their energy on the way through the detector. As a generator-level prescription to get some measure of how big an improvement this will make, we assume that neutral pions are perfectly measured, while no other hadrons are measured at all. In addition, we multiply all π^0 energies by a factor of three to arrive at an estimate of the total hadronic energy in the forward region.

In addition to extending our angular coverage, we can use additional kinematic variables of the final state to improve our W measurement. Defining the light-cone components of the particle momenta $p_\pm \equiv E \pm p_z$ we can write the invariant mass of the hadronic system as

$$W^2 = \left(\sum_i p_{i+} \right) \left(\sum_i p_{i-} \right) - \left| \sum_i \vec{p}_{i\perp} \right|^2, \tag{9}$$

where i runs over all hadrons. Using energy-momentum conservation (and neglecting the virtuality of the target photon) we can get some of the terms in Eq. 9 from the scattered electron, to define

$$W_{\mathrm{rec}}^2 \equiv \left(p_{e+} - p_{e'+} \right) \left(\sum_i p_{i-} \right) - \left| \vec{p}_{e'\perp} \right|^2. \tag{10}$$

This is equivalent to the well-known Jacquet-Blondel idea in photoproduction [25] except for the inclusion of the transverse momentum component. The sum over i now runs over hadrons in the central region, $|\cos\theta| < 0.97$, and π^0s in the forward region, $0.97 < |\cos\theta| < 0.9996$, and we include an extra factor of three for the forward π^0s.

Using Eq. 10 has two advantages over the naïve method of just using the invariant mass of detected hadrons. Firstly, the detector resolution enters as the product of hadronic and leptonic resolutions, rather than as hadronic-squared which, since the leptonic resolution is usually much better than the hadronic, gives improved overall resolution. Secondly, the effect of missing particles in the current direction $\theta \sim 0$ is minimized, because they give a negligible contribution to $E - p_z$. This, in addition to the inclusion of forward π^0s, means that W_{rec} is much better correlated with the true W, as seen in Fig. 9a. Also the differences between the models is much smaller.

In anomalous events, the photon remnant typically has larger transverse momentum, which means that in such events the correlation between W_{vis} and W_{true} is higher, as is seen in Fig. 9b. The definition of anomalous is, however, not the same in all generators, and in HERWIG, where anomalous events are defined by having a large transverse momentum remnant, the differences are larger than in PYTHIA, where the remnant has larger transverse momentum only on average.

Finally in double-tag events, we have more accurate information about the target photon energy, and hence the $W_{\gamma\gamma}$, as is seen in Fig. 10. It may be possible to use such events to calibrate the unfolding procedure for single-tag events. However, care must be taken, as in double-tag events, the target photon is more off-shell and the fraction of anomalous events are expected to be higher. See also sections 2 and 5 of the report from the "$\gamma\gamma$ Physics" [1] working group for more discussions of double-tag events.
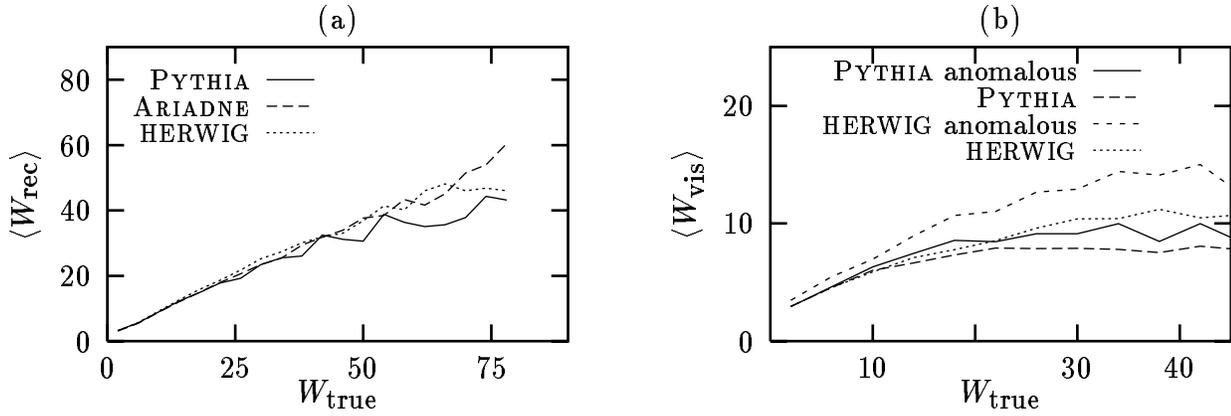
Figure 9: (a) The mean value of W_{rec} as a function of W_{true} at LEP 2 as predicted by different generators. (b) The mean value of W_{vis} for anomalous and normal events as a function of W_{true} at LEP 2 as predicted by different generators.
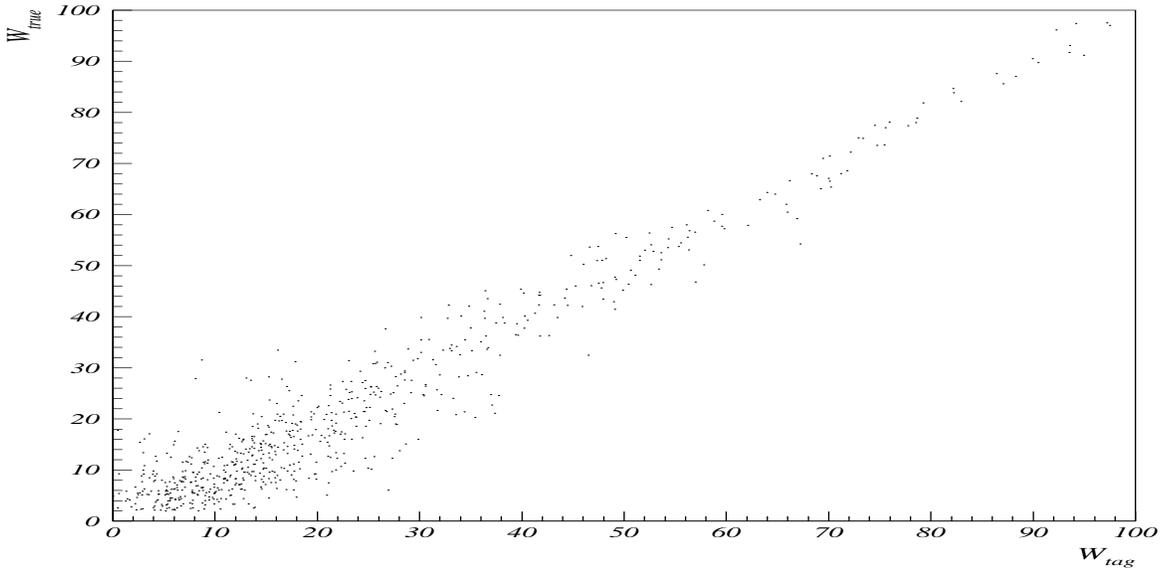

Figure 10: Scatterplot of W_{true} vs. W_{tag} at LEP 2 as predicted by HERWIG for double-tag events after detector simulation.
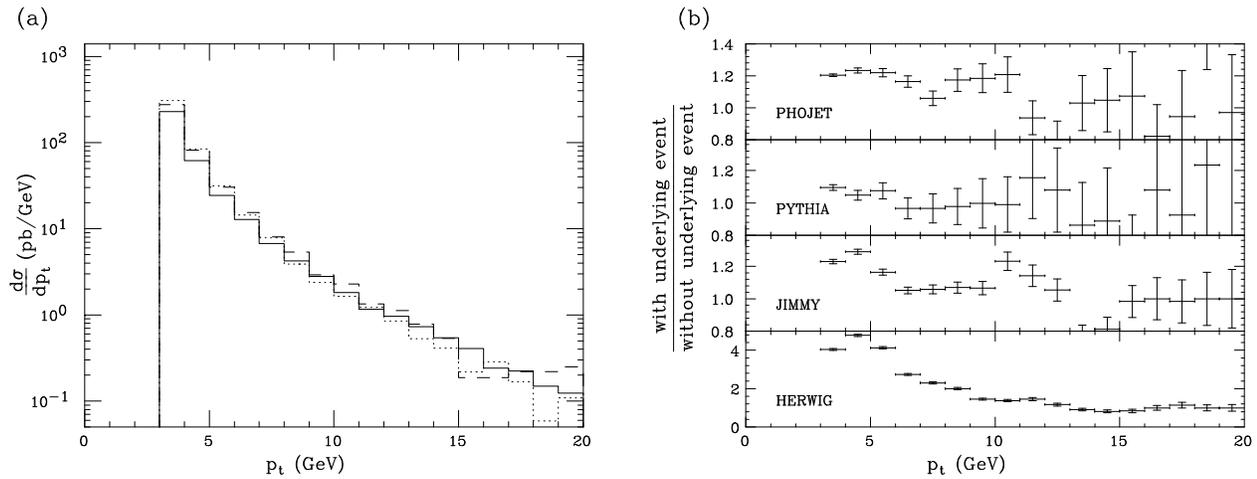
16

Figure 11: *The inclusive jet cross-section as a function of p_t according to HERWIG (solid),* PYTHIA *(dashed) and* PHOJET *(dotted), when all their underlying event models are turned off (a), and the relative changes when they are turned on (b). Errors shown come purely from the statistics of the Monte Carlo samples.*

3.4   High-$p_\perp$

Next-to-leading order QCD predictions are now available for both hadron and jet distributions in $\gamma\gamma$ collisions. Comparisons of data with these predictions are hoped to provide additional constraints on the parton content of the photon, particularly the gluon. However they apply to the partonic final state, consisting of at most three quarks or gluons, and cannot be compared to data without incorporating hadronization effects. For this to be done meaningfully, it is important to use general purpose QCD event generators, so that the parton level is as accurate a representation of the calculation as possible, while the hadronization is well-constrained by other reactions. Indeed the problems faced in $\gamma\gamma$ are almost identical to those in γp photoproduction at HERA, and we can expect that they will have been explored in detail by the time LEP2 analysis starts.

The hadronization effects can be broadly split into two groups: hadronization itself, and 'underlying event' effects, the latter coming principally from twice-resolved events in which the two photon remnants interact with each other in addition to the main scattering. Of course this separation is model-dependent, as hadrons described as coming from initial-state radiation in one model could be described as an underlying event in another, but it is a useful guide to where we expect the models to be more or less reliable. Hadronization itself is expected to be largely process-independent so models tuned to e^+e^- annihilation should give a reasonable description of data. Underlying event effects are much more poorly understood and the models are almost completely unconstrained at present. Their main effect is to spray additional transverse energy around the event, which can severely distort jet measurements, principally by adding extra transverse momentum to the jets. Because the jet spectrum is so rapidly falling, this increases the jet cross-section considerably at any given jet transverse momentum.

17

In Fig. 11, we show the inclusive jet cross-section, as a function of the jet transverse momentum. Jets are reconstructed using the CDF cone algorithm with a cone size of 1.0 and a minimum transverse momentum of 3 GeV, using all hadrons within the angular acceptance, $|\cos\theta| < 0.97$. We see reasonable agreement between PYTHIA, PHOJET and HERWIG when their underlying event and multiple scattering models are turned off. However, while all of them predict a significant increase with multiple scattering and the underlying event, there is little agreement about its size. It is worth pointing out that HERWIG's soft underlying event model produces far too big an effect to fit HERA photoproduction data, one of the motivations for incorporating the JIMMY multiple hard interaction model into HERWIG instead. Amongst the three other models the relative effect of multiple interactions is comparable to the differences between the models. It is clear that these effects must be understood before an accurate jet measurement can be made below about 10 GeV.

Of course the data itself can be used to study the effects and constrain the models. The jet energy profile is particularly sensitive to the underlying event, since perturbative radiation and hadronization are concentrated at the core of jets, while the underlying background is much more diffuse. Furthermore, since one expects the underlying event to mainly be important in the twice-resolved process, if we make a physical separation of direct and resolved photons we can test this picture. At HERA, a cut is made on x_γ, the fraction of the photon's light-cone momentum carried by the reconstructed jets [26]. In fact the HERA experiments define this in dijet events from the two hardest jets, while we propose a slightly different approach for $\gamma\gamma$ collisions: to use *all* the reconstructed jets, regardless of how many there are. Clearly when this fraction is close to 1 there can be no photon remnant, whereas when it is much smaller than 1 there must be one. The cut is typically set at around 0.7. For $\gamma\gamma$ collisions, we define a *pair* of momentum fractions by analogy, as

$$x_\gamma^\pm = \frac{\sum_{\text{jets}}(E \pm p_z)}{\sum_{\text{particles}}(E \pm p_z)}, \qquad (11)$$

where, following the discussion in section 3.3, we include three times the forward π^0 energy in the sum over particles, which significantly improves the measurement of the denominator of Eq. 11. We define the axes such that $x_\gamma^+ > x_\gamma^-$.

In Fig. 12, we show the E_T profile of the hardest jet in the central region, $|\eta| < 1$, where η is the jet rapidity. We only include the transverse energy within the azimuthal region $|\Delta\phi| < 1$, so in a two-jet event the E_T of the other jet should not contribute to the pedestal of this jet. We see that for the direct events, in which both light-cone momentum fractions are large so there is no significant underlying event, the multiple scattering makes very little difference. On the other hand, for twice-resolved events, in which both photons have remnants, it makes a lot more difference. The jet pedestal is sufficiently raised to increase a jet's transverse momentum by about 200 MeV. While this may not seem a large shift in absolute terms, the jet cross-section actually decreases by about 25% in going from 3 to 3.2 GeV, giving rise to the correction predicted by PHOJET in Fig. 11b. Because of the strong correlation between the shape of the jet and the shift in the cross-section, it seems hopeful that the models can be constrained by data, to provide a reliable unfolding of these effects. Indeed this is already in progress at HERA.
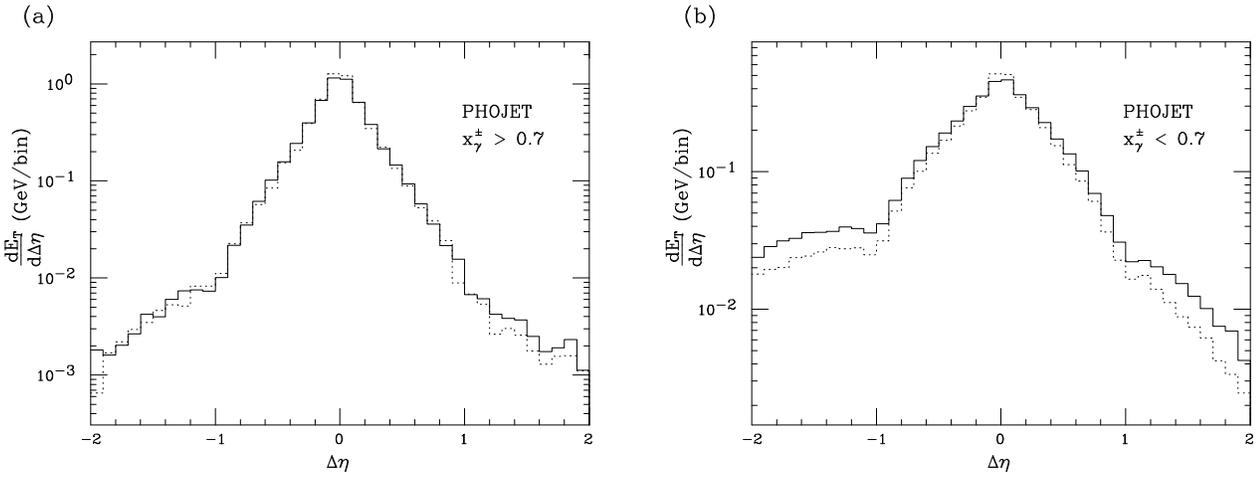
18

Figure 12: *The jet profile of central jets divided into (a) direct events and (b) double-resolved events according to a physical definition, as predicted by* PHOJET *with (solid) and without (dotted) multiple interactions.* $\Delta\eta$ *is the rapidity relative to the jet's, with the axes defined such that* $x_\gamma^+ > x_\gamma^-$ *such that there is always more of a remnant to the left than the right.*

Of course, one would like to make a more direct measurement of the nature of the underlying event, to differentiate between soft and multiple-hard interaction models. However it is extremely difficult to find event features that are unambiguous in this respect, as one's naïve picture of four jets in back-to-back pairs does not survive hadronization and realistic jet definition, so one is forced to look in the hard tails of distributions that are usually not well predicted anyway. Nevertheless, if direct evidence of multiple hard interactions could be found it would be extremely important for our understanding of photon and hadron collisions as a whole, and it is certainly worth continuing to search for such signals.

3.5   Heavy quarks

In this study we have compared five different generators of charm production in two-photon events: Vermaseren; PYTHIA; HERWIG; GGHV01 [27, 28]; and MINIJET [29]. All of these can generate the direct process, but only the last 4 the resolved process. For the comparison we chose the same parameters for each model: charm mass=1.7 GeV; minimum $c\bar{c}$ invariant mass=4.0 GeV; beam energy=85.0 GeV; and the GRV parton distribution set (for the resolved process).

We generated 10000 events with each program and compared the following distributions: scattered electron energy; final state invariant mass; energy, p_t and rapidity of the charm quark; p_t^2 of charm quarks with $\cos(\theta) < 0.9$ and energy > 2.0 GeV. In most cases the differences between the generators turn out to be rather small, so only a small selection are shown here (Figs. 13–15). Since they are so similar, we emphasize the differences by plotting the absolute distribution for only one generator (Vermaseren/PYTHIA for direct/resolved production) and
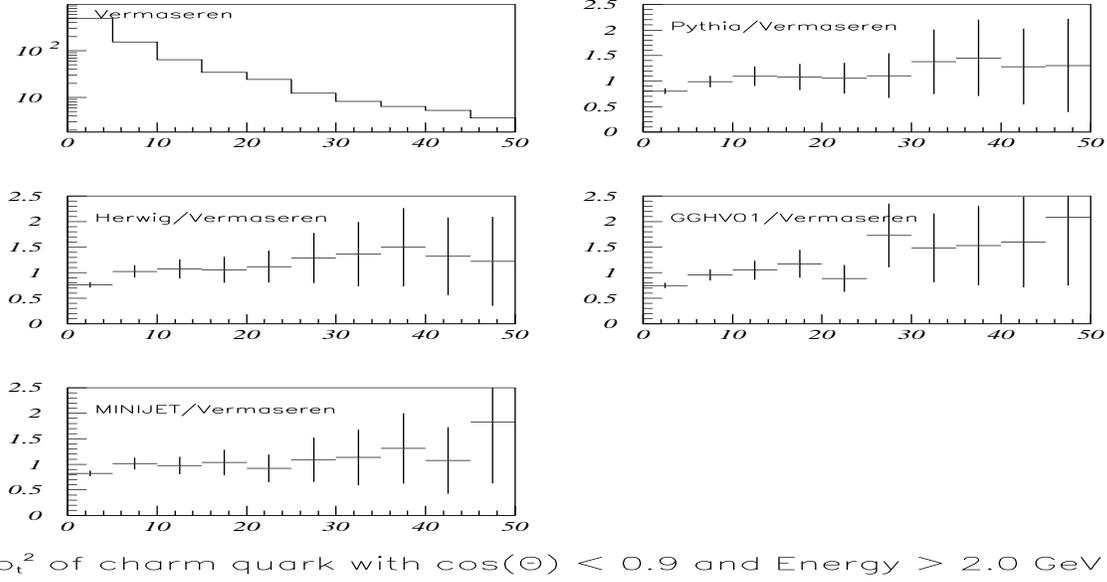
Figure 13: *Comparison of five generators of the direct production of charm quarks in two photon collisions. The top left histogram is the distribution for the Vermaseren generator. Other generators are shown as a ratio to the Vermaseren distribution in remaining plots.*

showing the results for the other generators as a ratio to it.

It can be seen that in the case of direct production the programs produce very consistent results. It should be noted that the Vermaseren generator is a full matrix element calculation while all the other generators involve a convolution of some version of the Equivalent Photon Approximation luminosity function with a cross-section for real photons. Thus it should be considered the correct answer to which the other calculations should be compared.

For the resolved process there is a larger variation between the generators. Unfortunately at this stage it is not clear which if any of these should be regarded as standard. The distribution that most clearly shows the differences is that of the rapidity of the charm quark (Fig. 15), where the MINIJET generator produces quarks that are more forward peaked, while GGHV01 produces more quarks in the central region. PYTHIA and HERWIG are fairly similar and lie somewhere in between.

Experimental charm measurement is generally restricted to the central region, with rapidity less than about 2. In Table 2, we show the selection efficiency of an imaginary experiment with 100% tagging efficiency for all charm quarks within the acceptance cuts, $\cos(\theta) < 0.9$ and $p_\perp > 2.0$ GeV. The differences in the rapidity distribution for resolved events are directly reflected in the selection efficiencies. One can see that an experiment using MINIJET to correct their data would 'measure' a resolved cross-section almost a factor of two larger than one using GGHV01, with PYTHIA and HERWIG lying between the two. It is therefore clearly a

20

Figure 14: *Comparison of four generators of the production of charm quarks via the single resolved process in two photon collisions. The top left histogram is the distribution for the* PYTHIA *generator. Other generators are shown as a ratio to the* PYTHIA *distribution in remaining plots.*
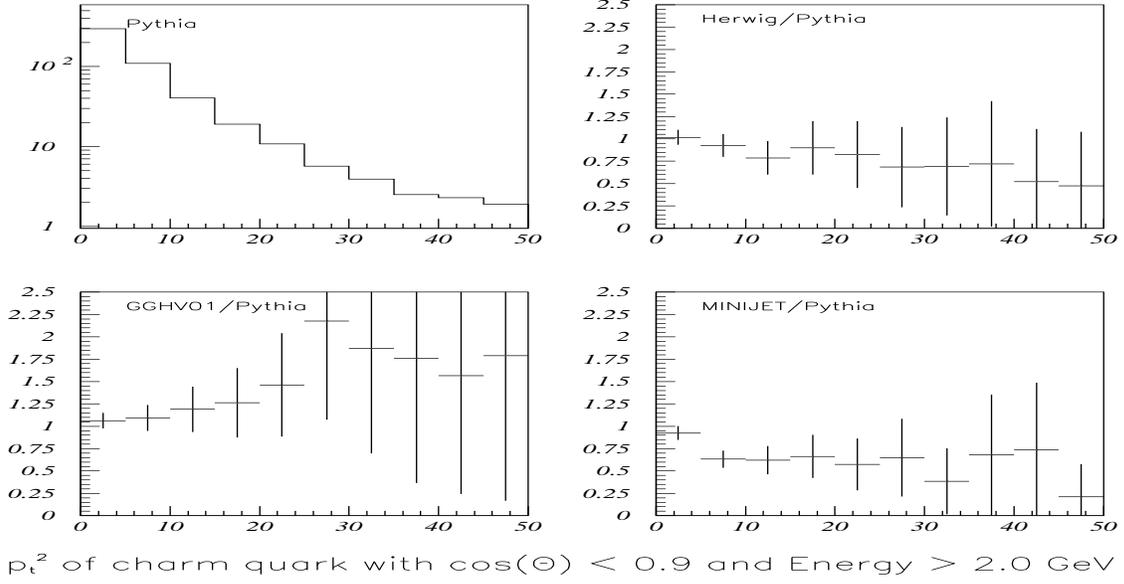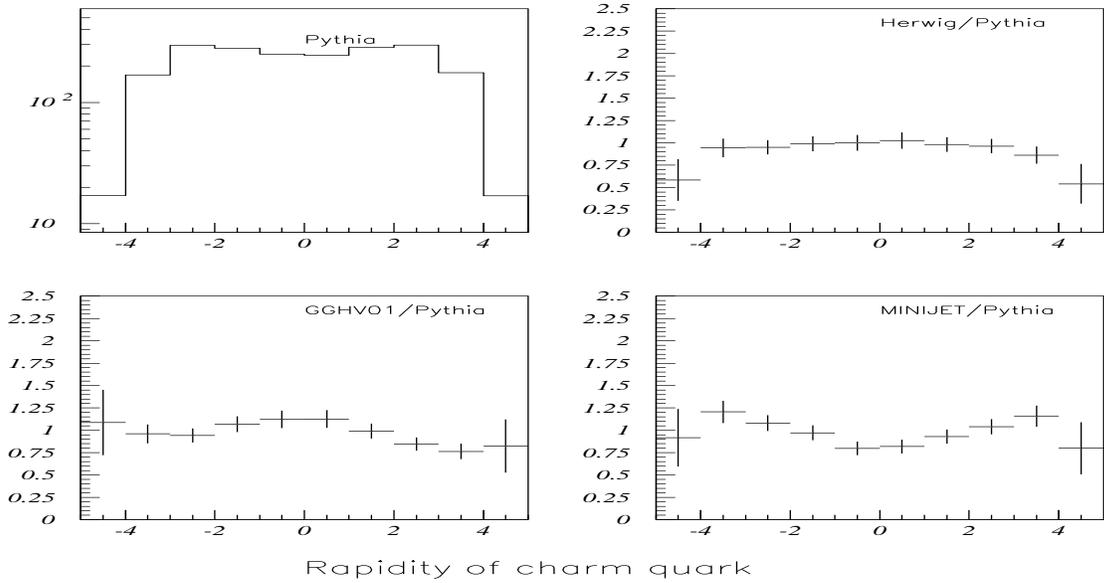

Figure 15: *Comparison of four generators of the production of charm quarks via the single resolved process in two photon collisions. The top left histogram is the distribution for the* PYTHIA *generator. Other generators are shown as a ratio to the* PYTHIA *distribution in remaining plots.*

21

Generator	Direct	Resolved
Vermaseren	42	-
GGHV01	39	28
PYTHIA	39	24
HERWIG	40	21
MINIJET	37	16

Table 2: *Percentage of events passing 'acceptance' cuts.*

high priority to understand where these differences arise and in particular whether the spread represents a genuine uncertainty in the measurement or is simply an indication that we should not trust one or some of the models. Unfortunately little progress has been made with this during the workshop.

Comparisons with data for the event features, rather than just the total cross-section, should also help to resolve this discrepancy. Within the limited statistics (33 events) Aleph found that GGHV01 gave a better description of data than the Vermaseren generator alone [27].

4   Description of programs

In this section we detail some of the event generators for $\gamma\gamma$ physics, concentrating mainly on those in which there has been significant development during this workshop. Other programs are commented on and described briefly in section 5.

4.1   Ariadne

Version: 4.07 of 15 August 1995 [30]
Author: Leif Lönnblad
                  NORDITA, Blegdamsvej 17,
                  DK 2100 Copenhagen Ø, Denmark
                  Phone: + 45 – 35325285
                  E-mail: leif@nordita.dk
Program size: 12839 lines
Program location: http://surya11.cern.ch/users/lonnblad/ariadne/

The ARIADNE program implements the Dipole Cascade Model (DCM) for QCD cascades [31,32]. In this model the emission of a gluon g_1 from a $q\bar{q}$ pair created in an e^+e^- annihilation event can be described as radiation from the colour dipole between the q and $\bar{q}$. A subsequent emission of a softer gluon g_2 can be described as radiation from two independent colour dipoles,

one between the q and g_1 and one between g_1 and $\bar{q}$. Further gluon emissions are given by three independent dipoles etc. In this way, the end result is a chain of dipoles, where one dipole connects two partons, and a gluon connects two dipoles. This is in close correspondence with the Lund string picture, where gluons act as kinks on a string-like field stretched between the $q\bar{q}$ pair.

Further details of how ARIADNE generates the QCD cascade in e^+e^--annihilation can be found in Ref. [30] and elsewhere in these proceedings [2]. Here only the parts relevant for eγ DIS and high-$p_\perp$ $\gamma\gamma$ is presented.

The treatment of DIS is very similar to e^+e^- [33] gluon emission is described in terms of radiation from the colour dipole stretched between the quark, struck by the electroweak probe, and the photon remnant. The difference is that, while q and $\bar{q}$ are both point-like in the case of e^+e^-, the photon remnant in DIS is an extended object. This results in an extra suppression of radiation in the remnant direction.

The suppression depends on the transverse size of the remnant, which is taken to be inversely proportional to its intrinsic transverse momentum $k_{i\perp}$. In anomalous events where $k_{i\perp}$ is larger, the suppression is therefore smaller than in VMD–like events. Also in events where the target photon is significantly off-shell, the transverse size is taken to be the inverse of the maximum of $k_{i\perp}$ and the photon virtuality. Similarly in the case of events with $Q^2 \ll W^2$, where gluons may be radiated with transverse momentum larger than Q, also the struck quark may be treated as extended with a transverse size $\propto 1/Q$.

The DCM is evidently very different from conventional initial-state parton shower models. Tracing emissions "backwards" from the struck quark as in an initial-state shower, these would be unordered in transverse momentum, while in a program like PYTHIA these emissions would be ordered in falling transverse momentum. In the DCM, the transverse momentum of gluons far away from the struck quark, i.e. close to the remnant, can be much larger than in an initial-state parton shower.

The first emission in the dipole cascade is corrected to match the $\mathcal{O}(\alpha_S)$ matrix element for gluon emission. The gamma-gluon fusion diagram is, however, not yet included for the eγ DIS, because of technical difficulties in the current interface to PYTHIA.

The interface to PYTHIA, described in the report from the QCD generator group [2], also enables ARIADNE to generate high-$p_\perp$ $\gamma\gamma$ scattering. Here, PYTHIA is used to generate the hard sub-process. The outgoing partons and remnants are then connected with dipoles, which are allowed to radiate, restricting the transverse momentum of the emissions to be smaller than that of the hard interaction and treating all remnants as extended objects as in DIS.

For $\gamma\gamma$ it is also possible to run ARIADNE with PYTHIA using multiple interactions. However, this part of the interface is still preliminary, and more studies are needed.

4.2 GGHV01

Version:	Version 1.0 of 1/11/1994
Author:	M. Krämer, P. Zerwas (DESY),
	J. Zunft (formerly of DESY, no longer in HEP) and
	A.Finch,
	School of Physics and Materials,
	University of Lancaster,
	Lancaster LA1 4YB United Kingdom
	Phone: (+44) 1524 593618
	E-mail: A.Finch@lancaster.ac.uk
Program size:	Interface routines:1148 lines
	Physics routines: 2639 lines
	Integration package (BASES): 4432 lines
Program location:	ftp://lavhep.lancs.ac.uk/

GGHV01 was developed by the above authors as a Monte Carlo implementation of the calculation in Ref. [28] of heavy flavour quark production in gamma gamma collisions at next to leading order. It can either produce direct or single resolved events at a range of beam energies, but is restricted to real photons only.

The program is not a complete NLO generator. It does generate the $2 \rightarrow 3$ process according to the NLO matrix elements, which is cut off against soft and collinear divergences. The remaining events are, however, approximated with $2 \rightarrow 2$ processes generated only to leading order, but rescaled so that the total NLO cross-section is reproduced.

During the initialization stage the routine `FANDK` calculates the factor by which the $2 \rightarrow 2$ process should be increased to achieve the correct cross-section. In order to do this it needs to know beforehand the total cross-section. This it finds from a parameterization of the total cross-section from Ref. [28]. This is a quick method but less flexible than recalculating the total cross-section from scratch. The latter approach may be adopted in a later version. The chief criticism of this approach is that there is just one global correction factor whereas a more sophisticated approach would be to calculate a different factor for different regions of phase space.

The main event generation loop uses the coupled routines BASES and SPRING [34] which together constitute a general purpose integration and event generation package. The input to both routines is a function to be integrated as a function of n random variables. In this case the routine `GENHVY`. This routine uses the input random numbers to first pick whether to generate a 2 or 3 body event, it then calculates the fraction of the energy of the incoming beam electrons taken by each photon. In the resolved photon case the fraction of the photon's energy taken by a gluon is also found using the Glück Reya and Vogt next to leading order parton distribution functions [10]. Momenta for the outgoing particles are then chosen using the subroutine `RAMBO`. The weight for the event is found using routines based on the NLO calculation of Ref. [28]

multiplied by the phase space weight from RAMBO. The 2 body ('Born term') contributions is additionally scaled by the factor calculated in the initialization step as described above.

During the BASES stage the program first optimizes a 'map' of the function to provide efficient calculation, and then calculates the total cross-section (for GGHV01 this simply provides a check as the total cross-section is already known). During the SPRING stage the function is repeatedly called to generate unit weight events which are put in the LUJETS common for fragmentation by the LUEXEC routine from the JETSET package. The map generated by BASES is written out to a file, which means the program can later be run from the SPRING step only. In this case it reads back the map produced in a previous run and by simply varying the random number seed a fast event generation can be achieved..

4.3   GGPS1, GGPS2

Version:	1.0 [35]
Author:	T. Munehisa, K. Kato, D. Perret-Gallix
	Phone: +81-552208584 (TM), +81-333421264 (KK),
	+33-50091600, +41 22 7676293 (DPG)
	E-mail: munehisa@hep.esb.yamanashi.ac.jp,
	kato@sin.kogakuin.ac.jp, perretg@cernvm.cern.ch
Program size:	2213 (GGPS1) and 2841 (GGPS2) lines
Program location:	ftp://lapphp8.in2p3.fr/pub/keklapp/ggps/ggps.tar.gz

This generator simulates jet productions in two-photon process based on the leading-log (LL) parton shower (PS) technique [36]. Two cases are separately treated, namely, the deep inelastic scattering of the photon (GGPS1) and the scattering of two quasi-real photons (GGPS2) [35]. Both processes begin by the PS space-like evolution, then the hard scattering of partons takes place, followed by the time-like evolution of the final state partons.

The non-singlet quark distribution in the photon, $q_{NS}(x, Q^2)$, obeys [37]

$$\frac{dq_{NS}(x, Q^2)}{d \ln Q^2} = \frac{\alpha_s}{2\pi} \int_x^1 \frac{dy}{y} P_{qq}^{(0)}(x/y) q_{NS}(y, Q^2) + \frac{\alpha}{2\pi} k_{NS}^{(0)}(x), \qquad (12)$$

The inhomogeneous term, $k_{NS}^{(0)}(x)$, is proportional to $x^2 + (1-x)^2$. α is the QED coupling constant, the QCD coupling constant α_s is defined as: $\alpha_s(Q^2) = 4\pi/(\beta_0 \ln Q^2/\Lambda^2) = \alpha_0/(\ln Q^2/\Lambda^2)$ with $\beta_0 = 11 - (2/3)N_F$. N_F is the number of flavours. Eq. 12 can be brought into the integral equation

$$q_{NS}(x, Q^2) = \int_x^1 \frac{dy}{y} K_{NS}^{(0)}(x/y, \overline{s}) q_{NS}(y, Q_0^2) + \int_{Q_0^2}^{Q^2} \frac{dK^2}{K^2} \int_x^1 \frac{dy}{y} K_{NS}^{(0)}(x/y, \eta(K^2)) \frac{\alpha}{2\pi} k_{NS}^{(0)}(y), \quad (13)$$

where $\overline{s} \equiv \ln(\alpha_s(Q_0^2)/\alpha_s(Q^2)) = \ln(\ln(Q^2/\Lambda^2)/\ln(Q_0^2/\Lambda^2))$ and $\eta = \ln(\ln(Q^2/\Lambda^2)/\ln(K^2/\Lambda^2))$. The first term represents the vector meson dominant part (VMD) while the second corresponds

to the perturbative photon. Here $K_{NS}^{(0)}(x, \overline{s})$ is the QCD kernel function [38] defined by the inverse Mellin transformation

$$K_{NS}^{(0)}(x, \overline{s}) = \int_{r_0 - i\infty}^{r_0 + i\infty} \frac{dn}{2\pi i} x^{-n} e^{\alpha_0 d(n)\overline{s}}, \tag{14}$$

where $d(n)$ is the moment of $P_{qq}^{(0)}(x)/(2\pi)$.

The singlet distribution is handled in the similar manner.

Due to the inhomogeneous term in Eq. 12, the total energy is conserved *only if* the photon energy is included,

$$\int_0^1 dx x [\sum_f (q_f(x, Q^2) + \overline{q}_f(x, Q^2)) + G(x, Q^2)] = \int_{Q_0^2}^{Q^2} \frac{dK^2}{K^2} \frac{\alpha}{2\pi} \int_0^1 dx x k_{NS}^{(0)}(x). \tag{15}$$

In the generation the right-hand side is used as *the weight of the event.*

Let us summarize the main steps present in the algorithm generating the partons in the course of the evolution.

1. Selection of a Q^2.

2. Calculation of the energy of the VMD part (independent of Q^2) and of the energy of the perturbative photon part by using Eq. 15. The sum of these energies is used as the weight of the event.

3. Selection of the actual process, either VMD or perturbative photon, according to the ratio of energies.

4. If VMD is chosen, the usual QCD evolution from Q_0^2 (the cut-off momentum) to Q^2 is performed.

5. In the case of a perturbative photon, the virtual mass squared K^2 according to the probability dK^2/K^2 is determined. Then the flavour of the partons are selected according to the ratio of charges squared.

6. For each quark or anti-quark, the usual QCD evolution from K^2 up to Q^2 is performed.

This algorithm is common to the deep inelastic photon scattering and to the two quasi-real photon scattering with large p_T^2. The hard scattering parts are, however, different. In quasi-real photon collision the initial states q-q, q-$\overline{q}$, q-G, G-G, q-γ G-γ and γ-γ are taken into account for the hard scattering, although in the virtual-quasi-real case only the γ^*-q and γ^*-G subprocesses are considered.

The reference cross-section used to select events is the differential cross-section:

$$d\sigma^0/dp_T^2 = \pi/p_T^4. \tag{16}$$

26

The ratio of the hard cross-section to Eq. 16 is counted as the weight of the event. The argument of α_s in the hard cross-section is set to be p_T^2, because there are some processes whose cross-section is dominated by the t-channel contribution. After the time-like evolution of the produced partons has been performed, the energy of the initial photons is fixed and thus the four-momenta of all partons are determined.

Events are generated with a weight whose maximum is unknown at the beginning of a run. A maximum value is arbitrary fixed by the user, overweight events are rejected and counted. At the end of the run, if the number of overweight events is too large, compromising the generation accuracy, the user must increase the maximum weight, reducing consequently the generation efficiency.

Finally the generated partons are hadronized following the JETSET [39] mechanism. Colour flows are properly matched and adopt the JETSET definition. Two types of colour singlet exist: a string beginning and ending with quarks possibly embedding one or many gluons or a closed colour loop of gluons.

4.4 HERWIG

Version: 5.8d of October 1995 [40] (and 5.9 of December 1995)
Authors: G. Marchesini[1], B.R. Webber[2], G. Abbiendi[3], I.G. Knowles[4],
                      M.H. Seymour[5], L. Stanco[3]
                      [1]Dipartimento di Fisica, Universita di Milano.
                      [2]Cavendish Laboratory, University of Cambridge.
                      [3]Dipartmento di Fisica, Universita di Padova.
                      [4]Department of Physics and Astronomy, University of Glasgow.
                      [5]Theory Division, CERN.
                      E-mail: webber@hep.phy.cam.ac.uk, knowles@v6.ph.gla.ac.uk,
                      seymour@surya11.cern.ch.
Program size: 15500 lines
Program location: http://surya11.cern.ch/users/seymour/herwig/

HERWIG is a general-purpose QCD Monte Carlo event generator for simulating **H**adron **E**mission **R**eactions, **W**ith **I**nterfering **G**luons. Its general design philosophy is to provide as complete as possible an implementation of perturbative QCD, combined with as simple as possible a model of non-perturbative QCD. It does this uniformly for a very wide range of processes, allowing the parameters to be fitted in one reaction, principally e^+e^- annihilation, and applied to other reactions. Although HERWIG has been capable of simulating $\gamma\gamma$ collisions for some time, there were many technical deficiencies, which practically prevented experiments from using it. Many of these have been rectified during the workshop, resulting in the preliminary versions 5.8a, 5.8c and 5.8d. However work is still ongoing, and some of the features described below will not be available until the full version release towards the end of this year. Since

much of HERWIG is described in Ref. [2], we concentrate on the additional features relevant to $\gamma\gamma$ collisions here. Original references can be found in Ref. [40].

Event generation proceeds much like the general case described in the introduction. The equivalent photon approximation (EPA) is used, correctly generating the P^2 dependence. Since this means that the photons no longer collide head-on, they are boosted to their centre-of-mass frame, where the remainder of the event generation is performed. At the end of the event they are automatically boosted back to the lab frame.

Since the user can control the P^2 range generated (through the variables Q2WWMN and Q2WWMX), it is in principle possible to generate all event classes using the EPA. However, to provide a more accurate description of high-Q^2 tagged events, these are described as deep inelastic scattering, e$\gamma \to$ e+hadrons including the full electron kinematics, rather than as $\gamma^*\gamma \to$hadrons using the EPA.

The treatment of deep inelastic lepton-photon scattering is essentially identical to that of lepton-hadron, except for the inclusion of the point-like photon-quark coupling in the initial-state parton shower. The hard process is generated as eq $\to$ eq according to whichever parton distribution function is selected from PDFLIB. This is controlled by the variables AUTPDF and MODPDF, which hold the 'author group' and set number respectively, for example GRVph and 3 for the leading-order photon set of Glück, Reya and Vogt.

The outgoing quark produces a parton shower exactly like that in the final state of e$^+$e$^-$ annihilation, described in Ref. [2]. The incoming quark also produces a parton shower, which is generated using the 'backward evolution' algorithm. One can imagine this as an evolution in the factorization scale from the large scale of the hard process down towards zero — as it is reduced, more and more radiation is resolved, i.e. transferred from the evolution of the parton distribution function to the coefficient function. The inhomogeneous term in the evolution equation corresponds directly to the addition of a $\gamma \to$ q$\bar{\text{q}}$ vertex, which is straightforwardly included by considering the photon to be an additional parton type with a delta-function distribution. This results in a dynamic separation of events into point-like and hadronic. At small and medium x values ($x \lesssim 0.3$), this separation is similar to that made in the input distribution functions, demonstrating the self-consistency of the backward evolution algorithm, but at large x it becomes increasingly different from them, classifying almost all large-x events as hadronic, whereas most distribution function sets classify them as point-like. The difference can be traced to the fact that HERWIG uses a cutoff in transverse momentum to separate the perturbative and non-perturbative regions, whereas the distribution functions make a cut on the virtuality of the internal line. At large x, the two differ by a factor of $(1 - x)$ giving large differences in the separation scales. While it could be argued that transverse momentum is a more physical scale to use, as in the FKP model, a more conservative approach is to simply say that this indicates a region of uncertainty, and any analysis that relies on the classification of this large x region into the two components should be considered highly model-dependent.

All partons produced by the initial-state cascade undergoing further parton showering just like any other outgoing parton.

Colour coherence is as important in initial-state cascades as it is in the final state. However it is less well understood and only an approximate treatment is implemented in HERWIG. At large x, all emitted gluons must be soft, the emission pattern is identical to a final state dipole, and the emission is angular-ordered. At small x, rather than restricting soft gluon momenta, we actually 'look inside' the soft gluons, resulting in a different coherence structure. At 'fairly small' x, this can be approximated by imposing transverse momentum ordering, which is how it is implemented in HERWIG, but at very small x the correct approach is to use angular ordering and modified emission probabilities. Although this has never been implemented as a full Monte Carlo event generator, a partial implementation was discussed in Ref. [41] and shown to give similar results to the HERWIG algorithm at the x values expected at LEP 2 or even HERA. The actual evolution variable used by HERWIG smoothly interpolates the two regions.

Just as in e^+e^- annihilation, HERWIG is not capable of covering the whole of phase-space with its parton shower emission. This is corrected using the methods proposed in Ref. [42], which ensure that the *hardest* emission (which is not necessarily the first owing to the ordering of opening angles) agrees with the exact matrix element (the sum of higher-order resolved, $g \rightarrow q\bar{q}$, $q \rightarrow qg$, and point-like, $\gamma \rightarrow q\bar{q}$). It is worth noting that azimuthal correlations [1] are correctly included within the 'dead-zone' region of x_p and z_p defined in Ref. [43], but not within the parton shower itself.

After the parton cascade, the system is hadronized according to the cluster model. For outgoing partons, this is identical to e^+e^- annihilation, described in Ref. [2], but for hadronic events, the photon remnant is treated specially. It is given a limited transverse momentum of width `PTRMS`, and the cluster that contains it is given a Gaussian mass-squared distribution, resulting in a limited p_t spectrum of produced hadrons, as expected for such a soft object. An 'underlying event' model is provided, which increases the energy released during the break-up of the remnant, but it seriously overestimates HERA data on DIS at small x, and it is recommended that it be switched off by running process `IPROC=19000` rather than `9000`[1].

Untagged and low-Q^2 tagged events are generated using the equivalent photon approximation to split both beams to photons. One hard process type is selected from those listed in Ref. [2]. At present there is no facility to mix events of different types in the same run, although it is clear that this would improve the utility of the program and it is a planned improvement. Events are generated according to the leading order matrix elements for $2 \rightarrow 2$ scattering, and initial-state and final-state showers are added exactly as in deep inelastic scattering. Another current problem is that the phase-space cuts accessible to the user are completely different for direct and resolved processes, making it difficult to generate both uniformly. Fixing this is another planned improvement.

In all event classes except deep inelastic scattering, it is recommended that the soft underlying event be selected. This models the collision between the photon remnants as a soft hadron-hadron scattering, which produces a uniform rapidity plateau of extra hadrons on top

---

[1]This applies to versions 5.8d onwards. In earlier versions, the two processes would be expected to bracket the correct result.

of those from the perturbative event. This is based on the UA5 minimum bias model, and is essentially just a parametrization of data. The soft VMD scattering process, `IPROC=8000`, uses the Donnachie-Landshoff cross-section and generates events as in the soft underlying event.

As discussed earlier, one would expect multiple hard scattering to be an important effect in untagged $\gamma\gamma$ collisions at LEP 2. Its contribution to the underlying event is also a major source of uncertainty in the measurement of jets at HERA and it is important to have several different models of it, to get some estimate of the uncertainty in the predictions. Although such scattering is not included in HERWIG at present, there is an interface to the JIMMY Generator [44] (which can also be obtained from the web-page listed above). However, there is not yet a smooth transition between hard and soft multiple scattering, and JIMMY and s.u.e. should be considered mutually exclusive at present.

The default parameter set that comes with HERWIG is tuned to OPAL data in the case of parameters that affect e^+e^- annihilation, but are simply theoretically prejudiced guesses for the others. At present the HERA experiments are involved with tuning the additional parameters and these will be included in future releases, hopefully improving the predictivity for $\gamma\gamma$ physics.

4.5 PHOJET

Version:	1.04 of 20 October 1995 [45]
Author:	Ralph Engel
	Institute of Theoretical Physics
	University Leipzig
	Augustusplatz 10, D-04109 Leipzig, Germany
	Phone: + 49 – 341 - 97 32444
	E-mail: eng@tph200.physik.uni-leipzig.de
Program size:	31000 lines
Program location:	http://www.physik.uni-leipzig.de/~engel/phojet.html

PHOJET is a minimum bias event generator for hadronic pp, γp and $\gamma\gamma$ interactions. The interactions are described within the Dual Parton Model (DPM) [46] in terms of reggeon and pomeron exchanges. The realization of the DPM with a hard and a soft component in PHOJET is similar to the event generator DTUJET-93 [47, 48]. Regge arguments are combined with perturbative QCD to get an almost complete description of the leading event characteristics. Special emphasis is taken on diffractive and soft interactions. Soft and hard interactions are unitarized together leading to the possibility to have multiple soft and hard scatterings in one event.

In the following, some comments on LEP 2 specific aspects are given. In the model [45], the dual nature of the photon is taken into account by considering the physical photon state as a superposition of a "bare photon" and virtual hadronic states having the same quantum numbers as the photon. Two generic hadronic states $|q\bar{q}\rangle$ and $|q\bar{q}^\star\rangle$ have been introduced to describe the

hadronic piece of the photon. The low-mass state $|q\bar{q}\rangle$ corresponds to the superposition of the vector mesons ρ, ω and ϕ and a $\pi^+\pi^-$ background. The state $|q\bar{q}^\star\rangle$ is used as an approximation for hadronic states with higher masses. The physical photon reads

$$|\gamma\rangle = \sqrt{Z_3}\, |\gamma_{\text{bare}}\rangle + \frac{e}{f_{q\bar{q}}}\, |q\bar{q}\rangle + \frac{e}{f_{q\bar{q}^\star}}\, |q\bar{q}^\star\rangle. \tag{17}$$

The interaction of the hadronic states via pomeron/reggeon exchange is subdivided into processes involving only *soft* processes and all the other processes with at least one large momentum transfer (*hard* processes) by applying a transverse momentum cutoff $p_\perp^{\text{cutoff}}$ to the partons. On Born-graph level, for example, the photon-photon cross-sections is built up by: **(i)** soft reggeon and pomeron exchange, **(ii)** hard resolved photon-photon interaction, **(iii)** single direct interactions, and **(iv)** double direct interactions. The soft pomeron cross-sections is parametrized using Regge theory. The hard cross-sections are calculated within the QCD Parton Model using lowest order matrix elements. For soft processes, photon-hadron duality is assumed. The energy-dependence of the reggeon and pomeron amplitudes is assumed to be the same for all hadronic processes. Therefore, data on hadron-hadron and photon-hadron cross-sections can be used to determine the parameters necessary to describe soft photon-photon interactions.

The amplitudes corresponding to the one-pomeron exchange between the hadronic fluctuations are unitarized applying a two-channel eikonal formalism similar to Ref. [47]. The probabilities $e^2/f_{q\bar{q}}^2$ and $e^2/f_{q\bar{q}^\star}^2$ to find a photon in one of the generic hadronic states, the coupling constants to the reggeon and pomeron, and the effective reggeon and pomeron intercepts cannot be determined by basic principles. These quantities are treated as free parameters and determined by cross-section fits [45]. Once the parameters are fitted, the model allows for predictions on photon-photon collisions without new parameters.

The probabilities for the different partonic final state configurations are calculated from the discontinuity of the scattering amplitude (optical theorem). Using the Abramovski-Gribov-Kancheli cutting rules [49] the cross-section for graphs with k_c soft pomeron cuts, l_c hard pomeron cuts, m_c triple- or loop-pomeron cuts, and n_c double-pomeron are estimated. For pomeron cuts involving a hard scattering, the complete parton kinematics and flavours/colours are sampled according to the Parton Model using a method similar to Ref. [50], extended to direct processes. For pomeron cuts involving parton configurations without a large momentum transfer, the partonic interpretation of the Dual Parton Model is used: photons or mesons are split into a quark-antiquark pair whereas baryons are approximated by a quark-diquark pair. The longitudinal momentum fractions of the soft partons are given by Regge asymptotics [51]. One obtains for the valence quark (x) and diquark ($1 - x$) distribution inside the proton $\rho(x) \sim (1 - x)^{1.5}/\sqrt{x}$ and for the quark antiquark distribution inside the photon $\rho(x) \sim 1/\sqrt{x(1 - x)}$. For multiple interaction events, the sea quark momenta are sampled from a $\rho(x) \sim 1/x$ distribution. The transverse momenta of the soft partons are sampled from an exponential distribution in order to get a smooth transition between the transverse momentum distributions of the soft constituents and the hard scattered partons.

31

In diffraction dissociation or double-pomeron scattering, the parton configurations are generated using the same ideas described above applied to pomeron- photon/pomeron scattering processes. According to the kinematics of the triple- or loop-pomeron graphs, the mass of the diffractively dissociating systems is sampled from a $1/M_D^{2\alpha_{I\!P}(0)}$ distribution. The momentum transfer in diffraction is obtained from an exponential distribution with mass-dependent slope (see Ref. [45]). For the parton distributions of the pomeron, the CKMT parametrization with a hard gluonic component [52] is used. The low-mass part of diffraction dissociation is approximated by the superposition of high-mass vector mesons. In order to take into account the transverse polarization of quasi-elastically produced vector mesons, diffractively scattered ρ, ω and ϕ are decayed anisotropically.

Finally, the fragmentation of the sampled partonic final states is done by forming colour neutral strings between the partons according to the colour flow. In the limit of many colons in QCD, this leads to the two-chain configuration characterizing a cut pomeron and a one-chain system for a cut reggeon. In hard interactions the colour flow is taken from the matrix elements directly [53]. The leading contributions of the matrix elements give a two-chain structure which corresponds to a cut pomeron. The chains are fragmented using the Lund fragmentation code JETSET 7.3 [39].

In order to get the LEP 2 kinematics, the complete lepton-photon vertex for transversally polarized photons is simulated in the program. The lepton (anti-) tagging conditions can be specified by the user. However, in the model only photons with very low virtualities are considered at the moment. The extension to virtual (and longitudinally polarized) photons is in progress.

An example input file for a $\gamma\gamma$ run can be in found in the PHOJET manual [54].

4.6 PYTHIA/JETSET

Versions:	PYTHIA 5.720 of 29 November 1995 [39]
	JETSET 7.408 of 23 August 1995
Author:	Torbjörn Sjöstrand
	Department of Theoretical Physics
	University of Lund
	Sölvegatan 14A, S-223 62 Lund, Sweden
	Phone: + 46 – 46 - 222 48 16
	E-mail: torbjorn@thep.lu.se
Program size:	19936 + 11541 lines
Program location:	http://thep.lu.se/tf2/staff/torbjorn/

PYTHIA/JETSET is a general-purpose generator of high-energy particle physics reactions. An introduction and a survey of processes of interest for LEP 2 physics are found in the QCD generators section, while the full description is in Ref. [39]. Here only aspects specific to $\gamma\gamma$

physics will be summarized. These have been developed together with Gerhard Schuler, and are described extensively elsewhere [55,56].

To first approximation, the photon is a point-like particle. However, quantum mechanically, it may fluctuate into a (charged) fermion–antifermion pair. The fluctuations $\gamma \leftrightarrow q\overline{q}$ can interact strongly and therefore turn out to be responsible for the major part of the $\gamma\gamma$ total cross-section. The spectrum of fluctuations may be split into a low-virtuality and a high-virtuality part. The former part can be approximated by a sum over low-mass vector-meson states, customarily restricted to the lowest-lying vector multiplet. Phenomenologically, this Vector Meson Dominance (VMD) ansatz turns out to be very successful in describing a host of data. The high-virtuality part, on the other hand, should be in a perturbatively calculable domain. Based on the above separation, PYTHIA distinguishes three main classes of interacting photons: direct, VMD and anomalous.

For a $\gamma\gamma$ event, there are therefore three times three event classes. By symmetry, the 'off-diagonal' combinations appear pairwise, so the number of distinct classes is only six. These are:

1. VMD$\times$VMD: both photons turn into hadrons, and the processes are therefore the same as allowed in hadron–hadron collisions.
2. VMD$\times$direct: a bare photon interacts with the partons of the VMD photon.
3. VMD$\times$anomalous: the anomalous photon perturbatively branches into a $q\overline{q}$ pair, and one of these (or a daughter parton thereof) interacts with a parton from the VMD photon.
4. Direct$\times$direct: the two photons directly give a quark pair, $\gamma\gamma \to q\overline{q}$. Also lepton pair production is allowed, $\gamma\gamma \to \ell^+\ell^-$, but will not be considered here.
5. Direct$\times$anomalous: the anomalous photon perturbatively branches into a $q\overline{q}$ pair, and one of these (or a daughter parton thereof) directly interacts with the other photon.
6. Anomalous$\times$anomalous: both photons perturbatively branch into $q\overline{q}$ pairs, and subsequently one parton from each photon undergoes a hard interaction.

In a complete framework, there would be no sharp borders between the six above classes, but rather fairly smooth transition regions that interpolate between the extreme behaviours. However, at our current level of understanding, we do not know how to do this, and therefore push our ignorance into parameters of the model. From a practical point of view, the sharp borders on the parton level are smeared out by parton showers and hadronization. Any Monte Carlo event sample intended to catch a border region would actually consist of a mixture of the three extreme scenarios, and therefore indeed be intermediate.

The main parton-level processes that occur in the above classes are:
- The 'direct' processes $\gamma\gamma \to q\overline{q}$ only occur in class 4.
- The '1-resolved' processes $\gamma q \to qg$ and $\gamma g \to q\overline{q}$ occur in classes 2 and 5.
- The '2-resolved' processes $qq' \to qq'$ (where q' may also represent an antiquark), $q\overline{q} \to q'\overline{q}'$, $q\overline{q} \to gg$, $qg \to qg$, $gg \to q\overline{q}$ and $gg \to gg$ occur in classes 1, 3 and 6.
- Elastic, diffractive and low-$p_\perp$ events occur in class 1.

33

The notation direct, 1-resolved and 2-resolved is the conventional subdivision of $\gamma\gamma$ interactions. The rest is then called 'soft-VMD'. The subdivision in PYTHIA is an attempt to be more precise and internally consistent than the conventional classes allow.

The cross-sections for the above components are based on a number of considerations. The VMD×VMD ones are derived from a Regge theory ansatz, with a pomeron plus reggeon form for the total cross-section, plus parametrizations of elastic and diffractive components [57]. The other five cross-sections are obtained by a direct integration of parton-level cross-sections above lower cut-offs $k_0 \approx 0.6$ GeV for $\gamma \leftrightarrow q\overline{q}$ fluctuations and $p_{\perp\min}^{\text{anom}} = 0.7 + 0.17\log^2(1 + E_{\text{cm}}/20)$ [GeV] for QCD processes in the anomalous sector. The latter is a purely phenomenological fit based on consistency arguments in the γp sector. It does not include possible eikonalization effects, and would therefore change in a more complete treatment (studies under way). Taken all together, one obtains a reasonable description of the total $\gamma\gamma$ cross-section.

The program comes with several parton-distribution sets for the photon. The default is SaS 1D [9]. In view of the above event classification, the SaS sets have the advantage that the separation into VMD and anomalous parts is explicit.

Currently only real incoming photons are considered. Eventually PYTHIA should be extended to (moderately) virtual photons. A separate treatment exists of the DIS region, $e\gamma \rightarrow eX$, i.e. with one real and one very virtual γ, but this option is less well developed (especially for parton showers). Furthermore, the program does not yet generate the spectrum of real photons internally, i.e. it is easiest to run for a fixed energy of the $\gamma\gamma$ system. It is possible to use the varying-energy and weighted-events options of the program to obtain a reasonable photon spectrum, however.

Some main switches and parameters of interest for $\gamma\gamma$ physics are:
- `MSEL` selects allowed processes; a change to 2 would include also elastic and diffractive VMD events.
- `MSTP(14)` sets the $\gamma\gamma$ event class among the six possibilities listed above. The most useful option is `MSTP(14) = 10`, where the six classes are automatically mixed in the proper proportions. Note that some variables, such as `CKIN(3)`, differ between the event classes and therefore automatically are reset internally.
- `MSTI(9)` tells which event class the current event belongs to.
- `MSTP(55)` and `MSTP(56)` gives choice of parton-distribution set and library for the photon.
- `PARP(15)` is the k_0 scale, i.e. minimum $p_\perp$ for $\gamma \leftrightarrow q\overline{q}$ fluctuations.
- `CKIN(3)` sets $p_{\perp\min}$ scale of hard interactions; for `MSTP(14) = 10` only to be set when studying high-$p_\perp$ jet production.
- `PARP(81)` (alternatively `PARP(82)`, depending on `MSTP(82)` value) sets the $p_{\perp\min}$ scale of multiple interactions in VMD×VMD events.

34

5 Other generators

Most of the general-purpose QCD event generators described above have only become available for $\gamma\gamma$ physics during the last year or two. Therefore most existing analyses have used generators written specifically for $\gamma\gamma$ physics with little or no overlap with other processes. This means that they are extremely hard to test thoroughly, except on the very data they are used to unfold. Although of course the different programs have different strengths and weaknesses, they are mainly based on the same general design. In this section we describe it and make a few general comments on when and why it is expected to be adequate or inadequate.

The principle way in which the older programs differ from the QCD generators is the lack of a parton shower stage. A hard scattering is typically generated according to the leading order matrix element, often taking great care with their accuracy and including many effects that are not yet included in the QCD programs. The final state described by these matrix elements ranges from a simple quark-antiquark pair in the case of DIS to up to two jets and two remnants in the case of high-p_t scattering. These simple partonic states are then given directly to the JETSET program, which implements the Lund string fragmentation model.

It may at first sight appear that parton showers are a luxurious frill that can be added to the model to slightly improve event simulation, for example by including the small fraction of events in which a third jet accompanies the two hard jets in an event. However in the modern view of hadronization, they are an essential precursor to the confinement of partons into hadrons, which does not take place globally between the main few hard partons in an event but locally between nearby soft partons. It is only by adopting the latter view that one can have any expectation that the hadronization process is universal. Quite apart from these theoretical issues, as a practical issue it is certainly the case that the parameters of the string model need to be retuned to fit to data at different energies and in different reactions when it is not preceded by a parton shower, but that coupled with a parton shower a reasonable description of all current data can be achieved with a single parameter set. This alone is enough to mean that any model that uses string fragmentation without a parton shower should be considered descriptive rather than predictive.

In addition to their rôle in setting the initial conditions for the hadronization process, parton showers are crucial for determining certain event features, for example the hadronic final state of DIS at small x, where the predictions of a 'QPM model', i.e. hard matrix element plus string fragmentation were found to give an extremely poor description of the HERA data [58].

Another closely related difference between the two groups of programs is in the assumptions made about the photon structure function. The older programs generally make an FKP-like [59] separation into the point-like and hadronic parts, a scheme with strong physical motivation, but then neglect the QCD evolution in the hadronic part. While one might suppose that this is unimportant if we only use the event generator as an unfolding tool, this is not in fact the case because structure functions do not just evolve by themselves, they do so by emitting gluons, which have an effect on the structure of the hadronic final state. QCD not only predicts that

35

changing Q^2 changes the structure function, but also the features of the hadronic final state. This should therefore be included in any model used to unfold data.

One possible solution would be to incorporate parton showers into the existing programs. However this is far from straightforward, because the evolution of a shower is strongly dependent on its initial conditions, namely on how the hard partons were formed. For example in DIS, simply setting up a $q\bar{q}$ pair and calling JETSET with its final state parton shower option switched on will result in emission with transverse momenta up to $W/2$, producing far too much hadronic activity. The correct solution, roughly speaking, is that the current jet produces a shower with upper scale of order Q, the photon remnant produces one of order its p_t and the internal line produces an initial-state shower. There are additional complications in the high-p_t case as there are contributions that contribute to different event classes depending on their kinematics, so one must impose additional constraints on the parton shower in order to avoid double-counting. Eventually, one realizes that to build in all the relevant conditions, the parton shower has to know so much about the hard process that one ends up almost having to write ones own parton shower algorithm from scratch.

Should we therefore conclude that existing programs are wrong and existing analyses need to be redone? No, because in the kinematic regions explored so far they have several advantages. Firstly the range in W has been rather limited so that the move into regions in which parton showers and QCD effects become important has been limited. Secondly for reasonably low W, most of the hadronic event is actually seen in the detector, so the actual reliance on the models is rather small. Thirdly, this means that the models can be well constrained and tested by fitting to the majority of the event so that they are fairly predictive for the unseen remainder of it. Finally, and very importantly, the low energy range has many problems associated with it that are rather carefully treated in the dedicated generators, such as exact kinematics, target mass effects, higher order terms in the EPA and other polarization states of the photon. This is in contrast with the QCD programs, which were traditionally oriented towards the high energy limit and are only now starting to 'catch up' in their treatment of effects important at lower energy.

In conclusion, we would say that at pre-LEP energies existing programs are perfectly adequate. At LEP 1, they have proved sufficient for most tasks, but problems are beginning to become apparent. For example, in DIS if one studies the energy flow in the detector as a function of x_{vis}, similar to what is shown in Fig. 8, one obtains predictions that are reasonably insensitive to the shape of the structure function and hence can make a fairly stringent test of the model. Preliminary results seem to indicate that existing models already have problems [60]. One can fairly confidently predict that at LEP 2 these problems will be sufficiently severe that using the QCD models will become essential, both because of the huge leap to smaller x and higher Q^2 and simply because of the higher statistical precision that will require better control of systematic errors.

Below we give a few basic facts about some of the programs used at present.

36

5.1 DIAG36

Author: F.A. Berends, P.H. Daverveldt and R. Kleiss [14]
                      E-mail: t30@nikhef.nl

Program size: 4335 lines

Program location: CPC program library

DIAG36 is an event generator for the full set of QED diagrams for $e^+e^- \to e^+e^-f\bar{f}$, including all fermion masses. Phase-space generation can cover the whole kinematically-allowed phase-space, or cuts can be applied for typical single- or double-tagged configurations.

5.2 MINIJET

Author: A. Miyamoto and H. Hayashii [29]
                      E-mail:hayashii@naras1.kek.jp

The MINIJET program generates the direct and the resolved photon events in two-photon processes of e^+e^- collisions. It calculates the cross-section of light- and heavy-quark production according to the EPA approximation for the photon flux and the leading-order matrix elements for the sub-process cross-sections. It uses the BASES program for the cross-section calculation and SPRING for the generation of four-momenta of final state partons. The generated parton are hadronized using the JETSET program. It has been used in the analysis of two-photon data by the TOPAZ group and in background studies for the JLC. Multiple interactions are not included in the program.

5.3 PC

Author: F.L. Linde [13]
                      E-mail: z66@nikhef.nl

The PC program generates two-photon events according to Eq. 2. It provides event generation of fermion pairs and resonance states in phase space of up to 4 final state particles with many dominant resonant states. The form factor is chosen between ρ, π, and J/ψ poles. It provides a cross-section calculation of all terms in Eq. 2.

5.4 RESPRO

Author: E.R. Boudinov and M.V. Shevlyagin [18]
                   E-mail: BOUDINOV@vxcern.cern.ch

The RESPRO program generates explicitly the two-photon resonance in a very efficient way and calculates the cross-section according to Eqs. 3 and 7.

5.5 TWOGAM

Authors: S. Nova, A. Olshevski, T. Todorov [6]
                   E-mail: todorovt@vxcern.cern.ch

TWOGAM implements Eq. 2 exactly for leptonic final states and for the direct, QPM, component of quark production, including all helicity states and the exact $2 \rightarrow 4$ kinematics. Single- and double-resolved components are added to the transverse–transverse scattering cross-section according to any parton distribution function selected from PDFLIB, and include a simple P^2-suppression model. The resulting partonic states are hadronized by the Lund string model, as implemented in JETSET. The user can select from several different soft VDM scattering models.

5.6 TWOGEN

Author: A. Buijs, W.G.J. Langeveld, M.H. Lehto, D.J. Miller [19]
                   E-mail: buijs@fys.ruu.nl
Program size: 1800 lines
Program location: http://www.fys.ruu.nl/ buijs/twogen/twogen.for

TWOGEN samples the transverse-transverse luminosity function for real and virtual photons of the multiperipheral diagram. The events are then weighted with any user supplied cross-section $\sigma_{TT}(\gamma\gamma \rightarrow X)$ and chosen using a simple "hit or miss" sampling. Thus, for example, the program can generate according to a chosen F_2 or can produce resonances. Final state partons are fragmented using the Lund string model in JETSET.

5.7 Vermaseren

Author: J.A.M. Vermaseren [15]
                 E-mail: t68@nikhef.nl

The Vermaseren Monte Carlo has become the *de facto* standard calculation of $e^+e^- \rightarrow e^+e^-f\bar{f}$ via $\gamma\gamma$ collisions. It uses the subset of the exact $2 \rightarrow 4$ matrix elements in which the electron and positron lines do not annihilate (i.e. formally they apply to the process $e^+\mu^- \rightarrow e^+\mu^-f\bar{f}$ with equal electron and "muon" masses).

6 Conclusions

$\gamma\gamma$ physics at LEP 2 is virtually impossible without event generators. Not only are they needed for modelling detector effects, as in almost all high energy physics analyses, but also because in $\gamma\gamma$ collisions the energy of the incoming photons is generally unknown. This means that we need to reconstruct the basic parameters of events solely from final-state properties. Except for the simplest final states consisting of only a few particles, detailed understanding is presently only possible through models implemented in event generators.

During the course of this workshop, several general purpose QCD generators have been developed to better handle $\gamma\gamma$ and $e\gamma$ interactions, enabling us to use experience gained from experiments with e^+e^-, ep and pp collisions, where these programs have been used extensively. A lot more work needs to be done however. In contrast to the special purpose generators used so far in $\gamma\gamma$ physics, which in the case of high energy multi-particle production are less theoretically advanced, the general purpose ones have not yet been extensively confronted with available data. Such comparisons have already been started for γp data from HERA with promising results, and it is important that this is also done with LEP 1 $\gamma\gamma$ data in preparation for LEP 2.

References

[1] Report of the $\gamma\gamma$ physics working group, these proceedings.

[2] Report of the QCD event generator working group, these proceedings.

[3] V.M. Budnev, et al., *Phys. Rep.* **15** (1975) 181.

[4] G. Bonneau, et al., *Nucl. Phys.* **B54** (1973) 573.

[5] J.H. Field, *Nucl. Phys.* **B168** (1980) 477; **B176** (1980) 545; **B187** (1981) 585.

[6] S. Nova, A. Olshevski, T. Todorov, DELPHI Note 90-35 (1990).

[7] S. Frixione, et al., *Phys. Lett.* **B319** (1993) 339.

[8] H. Plothow-Besch, *Comput. Phys. Commun.* **75** (1993) 396.

[9] G.A. Schuler and T. Sjöstrand, *Z. Phys.* **C68** (1995) 607.

[10] M. Glück, E. Reya, A. Vogt, *Phys. Rev.* **D46** (1992) 1973.

[11] B. Andersson, et al., *Phys. Rep.* **97** (1983) 31.

[12] B.R. Webber, *Nucl. Phys.* **B238** (1984) 492.

[13] F.L. Linde, "Charm production in two-photon collisions", RX-1224 (LEIDEN), (1988) thesis.

[14] F.A. Berends, P.H. Daverveldt, R. Kleiss, *Nucl. Phys.* **B253** (1985) 421; *Comput. Phys. Commun.* **40** (1986) 271, 285, and 309.

[15] J.A.M. Vermaseren, *Nucl. Phys.* **B229** (1983) 347.

[16] M. Poppe, *Int. J. of Mod. Phys.* **1** (1986) 545.

[17] F. Low, *Phys. Rev.* **120** (1960) 582; P. Kessler, *Nuovo Cim.* **17** (1960) 809.

[18] E.R. Boudinov and M.V. Shevlyagin, DELPHI 95-49 PHYS 487.

[19] A. Buijs, et al., *Comput. Phys. Commun.* **79** (1994) 523.

[20] W. Thomé, et al., *Nucl. Phys.* **B129** (1977) 365.

[21] V. Blobel, Proc. CERN school of computing, Aiguablava, Spain, September 1984.

[22] G. d'Agostini, *Nucl. Instrum. Meth.* **A362** (1995) 487.

[23] OPAL Collaboration, R. Akers, et al., *Z. Phys.* **C61** (1993) 199.

[24] DELPHI Collaboration, P. Abreu, et al., CERN-PPE/95-87, June 1995 (to be published in *Z. Phys. C*).

[25] F. Jacquet and A. Blondel, "Proc. of the study for an ep facility for Europe", DESY 79/48 (1979) 391.

[26] ZEUS Collaboration, M. Derrick, et al., *Phys. Lett.* **B348** (1995) 665.

[27] ALEPH Collaboration, D. Buskulic, et al., *Phys. Lett.* **B355** (1995) 595.

[28] M. Drees, et al., *Phys. Lett.* **B306** (1993) 371;
M. Krämer, proceedings of the Photon 95 conference, Sheffield, UK.

[29] A. Miyamoto, H. Hayashii, KEK Preprint 94-204, to appear in *Comput. Phys. Commun.*

[30] L. Lönnblad, *Comput. Phys. Commun.* **71** (1992) 15.

[31] G. Gustafson, *Phys. Lett.* **B175** (1986) 453.

[32] G. Gustafson, U. Pettersson, *Nucl. Phys.* **B306** (1988) 746.

[33] B. Andersson, et al., *Z. Phys.* **C43** (1989) 625.

[34] S. Kawabata, *Comput. Phys. Commun.* **41** (1986) 127.

[35] T. Munehisa, et al., KEK CP-034, KEK preprint 95-51, ENSLAPP-A-522/95, LPTHE-Orsay 95/37, to appear in *Z. Phys. C*.

[36] R. Odorico, *Nucl. Phys.* **B172** (1980) 157;
G. Marchesini and B.R. Webber, *Nucl. Phys.* **B238** (1984) 1;
K. Kato, T. Munehisa, *Comput. Phys. Commun.* **64** (1991) 67.

[37] E. Witten, *Nucl. Phys.* **B120**(1977)189;
Ch. Berger and W. Wagner, *Phys. Rep.* **146** (1987) 1.

[38] K. Kato, Y. Shimizu, H. Yamamoto, *Prog. Theor. Phys.* **63**(1980)1295;
K. Kato, Y. Shimizu, *Prog. Theor. Phys.* **64** (1980) 703; **68** (1982) 862;
K. Kato, Y. Shimizu, H. Yamamoto, preprint, UT-370 (1982), unpublished.

[39] T. Sjöstrand, *Comput. Phys. Commun.* **82** (1994) 74;
T. Sjöstrand, Lund University report LU TP 95–20 (1995).

[40] G. Marchesini, et al., *Comput. Phys. Commun.* **67** (1992) 465.

[41] G. Marchesini and B.R. Webber, *Nucl. Phys.* **B386** (1992) 215.

[42] M.H. Seymour, *Comput. Phys. Commun.* **90** (1995) 95.

[43] M.H. Seymour, contribution gls0258 to the "27th International Conference on High Energy Physics", Glasgow, U.K., 20–27 July 1994.

[44] J.M. Butterworth, J.R. Forshaw, *J. Phys.* **G19** (1993) 1657;
J.M. Butterworth, J.R. Forshaw, M.H. Seymour, CERN–TH/95–82, in preparation.

[45] R. Engel, *Z. Phys.* **C66** (1995) 203;
R. Engel. "Multiparticle Photoproduction within the two-component Dual Parton Model", in preparation, 1995;
R. Engel, J. Ranft, "Hadronic photon-photon collisions at high energies", ENSLAPP-A-540/95 (hep-ph/9509373), 1995.

[46] A. Capella, et al., *Phys. Rep.* **236** (1994) 227.

[47] P. Aurenche, et al., *Phys. Rev.* **D45** (1992) 92.

[48] P. Aurenche, et al., *Comput. Phys. Commun.* **83** (1994) 107.

[49] V.A. Abramovski, V.N. Gribov, O.V. Kancheli, *Yad. Fis.* **18** (1973) 595.

[50] K. Hahn and J. Ranft, *Phys. Rev.* **D41** (1990) 1463.

[51] A. Capella, et al., *Z. Phys.* **C10** (1980) 249;
A.B. Kaidalov, *Phys. Lett.* **B116** (1982) 459.

[52] A. Capella, et al., *Phys. Lett.* **B343** (1995) 403;
R. Engel, J. Ranft, S. Roesler, **Phys. Rev. D52** (1995) 1459.

[53] H.U. Bengtsson, *Comput. Phys. Commun.* **31** (1984) 323.

[54] R. Engel, PHOJET manual, 1995.

[55] G.A. Schuler, T. Sjöstrand, *Phys. Lett.* **B300** (1993) 169; *Nucl. Phys.* **B407** (1993) 539.

[56] G.A. Schuler and T. Sjöstrand, in "Two-Photon Physics from DAΦNE to LEP200 and Beyond", World Scientific, Singapore, 1994, eds. F. Kapusta and J. Parisi, p163;
T. Sjöstrand, in "XXIV International Symposium on Multiparticle Dynamics 1994", World Scientific, Singapore, 1995, eds. A. Giovannini, S. Lupia and R. Ugoccioni, p221.

[57] G.A. Schuler and T. Sjöstrand, *Phys. Rev.* **D49** (1994) 2257.

[58] H1 Collaboration, I. Abt, et al., *Z. Phys.* **63** (1994) 377.

[59] J.H. Field, F. Kapusta, L Poggioli, *Phys. Lett.* **B181** (1986) 362; J.H. Field, F. Kapusta, L Poggioli, *Z. Phys.* **C36** (1987) 121; F. Kapusta, *Z. Phys.* **C42** (1989) 225.

[60] F. Kapusta, I. Tyapkin, N. Zimin and A. Zinchenko, DELPHI note in preparation.